QUARTERLY REPORT FOR

JULY 1996-OCTOBER 1996

STANFORD GEOTHERMAL PROGRAM

STANFORD UNIVERSITY

15 October 1996

1 INJECTION INTO VAPOR-DOMINATED RESERVOIRS

This project is being conducted by Program Manager Prof. Shaun D. Fitzgerald and Undergraduate Research Student Catherine Tsui-Ling Wang. In this study we are investigating liquid injection and vaporization within a porous medium and within a fracture. This work is being conducted in collaboration with Andrew Woods, University of Cambridge and Karsten Pruess, Lawrence Berkeley Laboratory.

During the last three months, work has continued on injection into superheated rough-walled fractures. Further analysis of previous experiments and those conducted during the last quarter appear to validate the numerical predictions that one may derive using conventional reservoir simulators such as TOUGH2.

We first report on the developments for modeling a propagating boiling front through a porous medium and then summarize the results obtained for injection into horizontal superheated fractures.

1.1 THE VAPORIZATION OF A LIQUID FRONT MOVING THROUGH A HOT POROUS ROCK

1.1.1 Introduction

The theoretical results presented in the previous quarterly report on the evolution of a boiling front propagating through a porous medium were based upon the premise that the liquid-vapor interface remained stable. However, Fitzgerald and Woods (1994) showed that if the fraction of liquid which boils is sufficiently high (>20% for typical geothermal reservoirs), then the interface may become unstable and break up into fingers.

Although the wavelength of disturbance with the fastest growth rate at the onset of instability may be determined from a full linear stability analysis, the nonlinear evolution of the interface is unknown. We plan to investigate how the morphology of the interface develops with time using a laboratory analogue system of injection into a geothermal

reservoir. Using the results obtained from the experiments we intend to derive scalings for the growth of the effective two-phase zone at the interface in order to model the system.

1.1.2 Development

The experimental apparatus is currently under construction. We have purchased a slab of Berea sandstone of 12 inches diameter and 1 inch thickness. The 500md sample is reportedly relatively homogeneous. A central injection port has been drilled in addition to twelve thermocouple wells. The apparatus will be sealed at the top and lower boundary using flexible epoxy, as in the previous experiments for liquid injection into a liquid-saturated cement-sand manufactured core. It is intended that experiments will be conducted with water in order that the evolution of the saturation profile within the core may be determined through the use of the X-Ray CT scanner. Previous experience suggests that large temperature variations can cause the apparatus to fail. As a result, we may elect to use a fluid of lower boiling point such as ether or alcohol to perform these experiments.

Simple scaling models for the growth of an effective two-phase zone have been developed for describing the solidification of various salts and metals. These propagating solid-liquid boundaries are also unstable and "mushy" zones develop at the interface between the liquid and solid. We hope to develop a similar technique to describe the growth of the two-phase zone following injection into a superheated geothermal system.

1.2 INJECTION INTO A HEATED FRACTURE

1.2.1 Introduction

This project is being conducted by Program Manager Prof. Shaun D. Fitzgerald, Undergraduate Research Student Catherine Tsui-Ling Wang and Dr. Karsten Pruess, Lawrence Berkeley Laboratory. In this study we are investigating liquid injection and vaporization within a fractured reservoir.

In the previous report we presented results of experiments being conducted in which liquid ether is injected into a horizontal rough-walled fracture. As liquid ether is injected into the apparatus, some of the ether boils. In the earlier experiments, it was observed that the edge of the two-phase zone propagated as an ellipse and that the front tended to pulse. We have now determined that the elliptical shape was a function of the deformation of the glass plates during the heating stage of the experiment. This problem has been overcome by the utilization of a different support mechanism for the apparatus at all stages of the experiment. We have successfully compared the experimental findings with numerical predictions based upon a version of TOUGH2 adapted to account for the properties of liquid ether rather than water. The study of injection into horizontal fractures has been completed and the next stage of the project will be to analyze the injection of liquid into a vertically-orientated fracture. We summarize below the results of

the project of injection into horizontal fractures which will be published in the Proceedings of the 18th New Zealand Geothermal Workshop.

1.2.2 Background

In the early stages of development of geothermal power for electricity, the separated brine or condensate which was produced was considered to be a waste disposal problem. In some cases the fluid was disposed of in a nearby river such as in Tibet and at Wairakei, New Zealand. Geothermal brine typically contains toxic substances such as arsenic and boron, and therefore it is not generally permissible nowadays to dispose of the fluid in this way. Injection of this fluid provides an alternative disposal mechanism, and deep reinjection in the peripheral areas of Onikobe, Japan (Horne 1982) and Palinpinon, Philippines (Harper and Jordan 1985) have been successful. Further strategic changes in the treatment of separated brine or condensate have arisen following significant pressure reductions in various reservoirs following their exploitation. Severe reduction in reservoir pressure is primarily caused by the net extraction of fluids. Hence, reinjection of reservoir fluid is now considered a major factor in the development plan for geothermal reservoirs since reinjection reduces the net fluid loss from the reservoir. In some cases additional liquid is being considered for injection in order to help maintain the reservoir pressure and provide a solution for the disposal of toxic waste. At The Geysers, construction has commenced on a $40m pipeline to transport treated waste water from Lake County to the reservoir in order to provide sufficient fluid for injection. Plans are also being considered for the injection at The Geysers of waste water from the city of Santa Rosa.

Experience has shown that in many cases, the injection of brine or condensate has helped reduce the pressure decline (Enedy, Enedy and Maney 1991; Goyal 1994). However, thermal breakthrough has occurred in some instances (Goyal 1994). Thermal breakthrough associated with large volumes of reinjected brine at Kakkonda caused a reduction in plant performance from 50MW in July 1979 to 37 MW in April 1981. Premature thermal breakthrough resulted from the fracture network linking various injection wells to some of the production wells. Cessation of injection into these particular injection wells enabled the power plant output to return to 41 MW by October 1981 (Nakamura 1981).

Theoretical treatments of fluid migration and heat transfer within geothermal reservoirs based upon porous medium type models are unable to account for the thermal degradation in production wells which arise due to cold water migrating through fractures. Some of the primary benefits of these type of models are that they are relatively simple to use and have been successfully compared with laboratory experiments (Fitzgerald and Woods. 1994; Woods and Fitzgerald 1996 1997). In a porous medium type model of cold water injection into a geothermal reservoir, the thermal front associated with the injected liquid lags behind the advancing fluid itself (Bodvarsson 1972; Pruess *et al*. 1987; Woods and Fitzgerald 1993). The analysis of injection into discrete fractures is more difficult to perform as a consequence of the three-dimensional heat and mass transfer which results. When liquid migrates along a fracture, conduction of heat along the axis of flow and perpendicular to the direction of fluid flow can be important. In situations where the

fractures are spaced sufficiently close together that the time for thermal diffusion between the fractures is much faster than the timescale of interest, the fractured system can be adequately described by an equivalent porous medium system (Bodvarsson and Tsang 1982; Pruess and Bodvarsson 1984). However, in many instances this is not the case and explicit modeling of the presence of fractures is required.

We have performed a series of laboratory experiments designed to test the theoretical treatments of liquid injection into liquid-dominated and vapor-dominated reservoirs (Bodvarsson 1972; Mossop 1996; Pruess *et al.* 1987). Experiments have been performed in which liquid was injected at a constant rate into an impermeable transparent glass-walled fracture. The temperature changes due to heat transfer were recorded using thermocouples and the migration of the front by video.
We first describe the experimental procedure, describing the problems encountered during liquid injection into liquid-saturated and superheated systems. We then discuss the heat transfer which occurs as liquid is injected into a rough-walled fracture and compare the results with the theoretical predictions. These results build upon the earlier experimental work of Fitzgerald, Pruess and van Rappard (1996).

1.2.3 Experimental Procedure

The fracture apparatus was constructed using two 18" diameter sheets of 3/4" thick toughened glass and two sheets of shower door glass. The shower glass sheets were glued to the toughened glass in order to increase the heat capacity of the glass bounding the fracture. It was important that the apparatus was made of transparent material in order that the migration of the front of injected water within the fracture could be followed. An injection port was drilled into the center of one of the fractures and a brass injection fitting was glued to the outer surface. The glass plates were laid on top of one another in order to create the fracture and the surface disparities formed the pathways for the migration of fluid. The plates were sufficiently heavy that the fracture remained at the same aperture for the flow rates used without the use of clamping devices.

The apparatus was laid horizontally and the fluid injected at either constant rate or pressure into the port from the base. For the experiments in which liquid was injected into a liquid-filled fracture deionized water was used as the working fluid. However, the experiments investigating boiling used ether since it has a considerably lower boiling point (34^{o}C at atmospheric pressure). In order to track the front of the injected fluid, a video camera was placed above the vessel and the injected fluid was died with ink. As the fluid migrated through the fracture the position of the front marked by the ink was clearly visible. In the case of liquid injection into a liquid-filled fracture, the ink front corresponded to the front of new fluid. However, in the case of boiling within the fracture, the ink front marked the leading edge of a two-phase zone since the dye was only soluble in the liquid phase. As a result, injected fluid existed ahead of the front as vapor. The evolution of the temperature profile within the fracture was recorded by using an array of thermocouples within the fracture. Although the leadwires were drawn across the fracture, no disturbance to the flow was observed. The thermocouples were connected

to a digital recorder and the temperatures recorded every 10s. A schematic diagram of the experimental set up is shown in Figure 1.1.

The investigation of the heat transfer between the rock and fluid was conducted by heating the apparatus overnight in an oven to temperatures varying between 50-90^{o}C. In order to analyze water injection into a liquid-filled fracture, the apparatus was contained in a water bath during the heating stage. The plates were then placed together and taken from the water bath in order to perform the experiment.

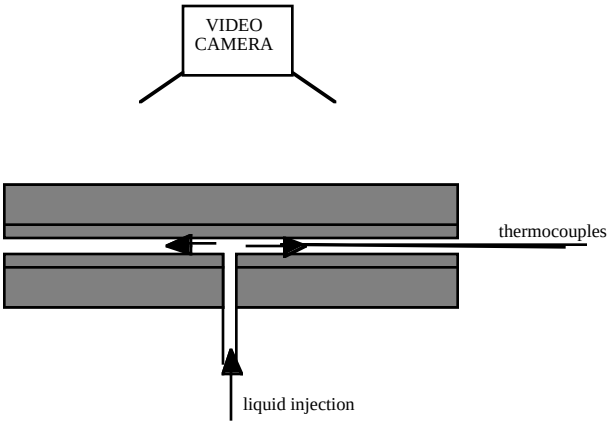

Figure 1.1 Schematic diagram of the apparatus. Liquid is pumped through the inlet port and migrates through the fracture spreading axisymmetrically.

The formation of air bubbles during the heating phase of the liquid-filled fracture experiments caused the front of newly-injected liquid to be irregular, with air trapped in the fracture by surface tension. In order to overcome this problem it was necessary to remove all air bubbles from the surfaces and pipes whilst the apparatus was in the water bath.

A further problem became apparent during the boiling experiments. During the initial series of experiments the leading edge of the two-phase zone was elliptical. This was found to be a consequence of the support mechanism for the glass plates. The glass plates tended to deform when heated overnight in the oven and supported at the edges. In order to prevent this, the support mechanism was altered and the boiling front propagated in a roughly circular manner in subsequent experiments.

1.2.4 Liquid-Filled Fracture

In this section we examine the injection of liquid into a liquid-filled fracture. We have conducted a series of experiments in which water of temperature 20 ^{o}C was injected at rates of 3, 6 and 10ml/min into a fracture bounded by rough-walled glass varying in temperature between 40-90^{o}C. Thermocouples were placed within the fracture at various distances from the inlet port. As liquid water was injected into the fracture, the temporal changes in temperature were recorded.

As liquid migrated through the fracture, the initially cold injected fluid became heated as heat was transferred from the fracture walls to the fluid. A theoretical model of the problem of injection into a liquid-filled fracture bounded by impermeable rock of infinite extent was investigated by Bodvarsson (1972). In his analysis, radial conduction of heat was considered to be negligible, the fluid was assumed to be well mixed across the fracture aperture and at the same temperature as the rock face, and the accumulation of heat by the fluid was ignored. In reality, the injected fluid accumulates heat and the cold zone which develops around the injection port is of greater extent than that predicted by Bodvarsson (1972). If one includes the effects of accumulation of heat by the fluid then one obtains the following expression for the temperature of the fluid as a function of radial distance r and time t (Mossop 1996)

$$\eta = erf\left(\xi\right) \tag{1.1}$$

where

$$\xi = \left(\frac{\Pi k r^2}{Q C_{pw} \sqrt{\kappa \left(t - \frac{\Pi h \rho r^2}{Q} \right)}} \right) \tag{1.2}$$

and k is the thermal conductivity of the rock (glass), Q is the injection mass flux, C_{pw} is the specific heat capacity of water, κ is the thermal diffusivity of the rock (glass), h is the fracture aperture and ρ is the density of water. η is the dimensionless temperature defined as

$$\eta = \frac{T - T_{inj}}{T_o - T_{inj}} \tag{1.3}$$

where T_{inj} is the temperature of the injected fluid and T_o is the initial temperature of the rock. This expression is valid only for intermediate times in which the conduction of heat in the radial flow direction may be neglected. Values used in the experiments were as follows: k=0.937W/mK, Q=5-10g/min, C_{pw}=4180J/kgK, κ=4.21e-7m^2/s, h=0.18mm and ρ=1000kg/m^3. The theoretical prediction for the variation of temperature η with dimensionless time ξ at a given distance from the injection port is shown by the solid line in Figure 1.2.

The data obtained from the experiments is also plotted in Figure 1.2. Each experimental set of observations are represented by different symbols. We find that the experimental results are in excellent agreement with the theoretical prediction even though the theory is only strictly valid for rock of infinite extent. In our experiments the glass sheets were 1.9cm thick. We thus expect that the cooling of the outer surfaces of the glass to become

important after a time of order (D^2/κ) where D is the thickness of the glass. Using the manufacturers value for the diffusivity κ =4.21e-7 m^2/s we find that the time which may elapse after taking the glass from the water bath before the effects of cooling become important is approximately 15 mins. All of the experiments were completed within this time frame.

A further possible discrepancy between the experimental results and theoretical predictions arose from the heat capacity of the brass injection port which is not included in the theory. The field scale equivalence of this is the additional heat transfer which occurs due to heat transfer along an injection well bore prior to the liquid entering a fracture. The additional heating of the fluid by the brass injection port was more significant during the early stages of the experiment. As the experiment proceeded the brass port cooled more rapidly than the extensive glass plates. As a result the discrepancies between the theoretical prediction (Mossop 1996) and experimental results are greatest for larger values of ξ (smaller values of time) where the measured temperatures are greater than the predicted values. The experiments therefore support the theory for times sufficiently long that the effects of well bore heat transfer are negligible.

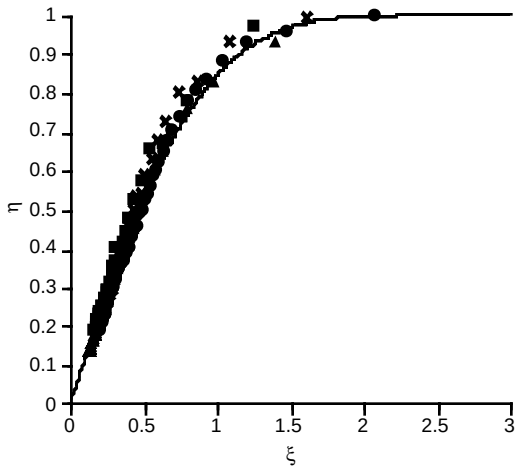

Figure 1.2 The variation of dimensionless temperature η as a function of the similarity variable ξ. The solid line represents the theoretical prediction and the symbols represent the results obtained from a series of experiments in rough-walled fractures.

1.2.5 Vapor-Filled Fracture

In numerous geothermal reservoirs, some of the fractures are filled with vapor rather than liquid. This can be the result of large scale depletion such as at Wairakei (Grant 1979), where a steam cap has formed, even though the fractures were originally liquid-filled. Alternatively, systems in which fractures are vapor-filled can occur naturally such as at The Geysers, Larderello and Kawah Kamojang. Injection of liquid into systems such as these is also conducted in order to provide pressure support for the production wells. As

the liquid migrates into the reservoir along fractures it is heated and a fraction of it boils. The newly generated vapor can migrate to production wells and lead to increased production. In addition to the increase in reservoir pressure, the productivity of the wells can improve since the newly generated vapor within the reservoir generally has a lower non-condensible gas content (Klein and Enedy 1989; Enedy *et al*. 1993). Thus, the power plant output per unit mass of extracted fluid can increase. The fraction of liquid which actually boils depends on the amount of heat which can be transferred to the fluid and the pressure within the fractured reservoir. A number of theoretical and laboratory studies of liquid injection into a superheated reservoir consisting of a porous rock have been conducted (Pruess *et al*. 1987; Woods and Fitzgerald 1993 1996 1997). These studies showed that the amount of heat which can be extracted from the rock and used for vaporization is a function of the extent of cooling which occurs at the vaporization front and the amount of heat which is conducted towards the point of injection. The laboratory experiments support the theoretical predictions for the evolution of the system as liquid flows into a vapor-filled porous medium type reservoir (Woods and Fitzgerald 1996). In this case, the heat required to overcome the latent heat of vaporization is supplied by the rock grains within the vapor-saturated thermal boundary layer immediately ahead of the liquid-vapor interface. However, in the case of a fractured system, the heat is supplied by conduction from the fracture walls perpendicular to the flow. In order that boiling may occur, the heat required to overcome the latent heat of vaporization must be supplied over a finite area. As a result, boiling has to occur over a broad two-phase zone rather than a sharp interface. This is in contrast to the case of injection into a porous medium at low degrees of superheat, where the liquid-vapor transition zone can be a narrow interface. However, it is similar to the case in which a porous medium type reservoir is sufficiently superheated that the propagating liquid-vapor interface may become unstable and break up into fingers (Fitzgerald and Woods 1994).

Having established that boiling must occur over a two-phase zone, it is of interest to determine how the temperature and liquid- and vapor-saturations vary with radial distance since the migration of cold liquid along a fracture can lead to premature thermal breakthrough at nearby production wells (Nakamura 1980). As liquid is injected into the fracture, we expect that the pressure will decrease monotonically away from the inlet port as fluid migrates into the far-field. After a period of injection we anticipate that the fluid within the fracture close to the inlet port will be liquid since the pressure is highest at this point and the rock closest to the injection point will have undergone the most cooling. In the far-field, we expect that the fracture will be filled with vapor at relatively low pressure and at a temperature close to the initial temperature of the rock. However, if the pressure is prescribed to decrease monotonically away from the inlet port and the boiling zone is to be of finite extent then the temperature must decrease within the boiling zone if steam and water are in thermodynamic equilibrium. In order to develop a quantitative model of this scenario we have used the TOUGH2 general purpose numerical code (Pruess 1991) for solving the coupled equations of heat and mass conservation in a fractured-porous type geothermal reservoir.

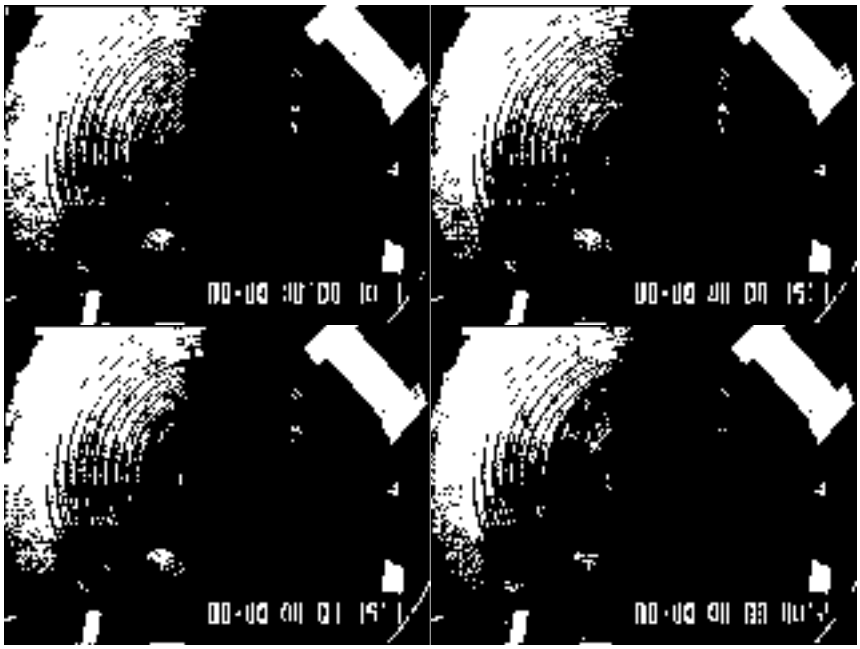

Figure 1.3 The spreading of dyed ether as it is injected at 20ml/min. The times shown correspond to times 10, 15, 75 and 180s after the onset of injection. The region of concentrated dye indicates the leading (front) edge of the two-phase boiling zone.

In addition we have conducted a series of experiments in which liquid ether was injected at rates of 10-20 ml/min into a horizontal rough-walled fracture in order to determine whether a two-phase zone does indeed develop as predicted. Ether was chosen as the working fluid since it boils at 34.5^{o}C at atmospheric pressure thereby enabling us to study the boiling process using fracture temperatures of 50-90^{o}C. In Figure 1.3 we show a series of photographs taken at various times during the course of one experiment as ether was injected at constant rate. As the ether migrated radially out into the fracture, a liquid zone developed close to the injection port. Ahead of this zone a two-phase region developed. The leading (front) edge of the two-phase zone is shown in Figure 1.3 by the region of concentrated dye. The orange dye used was only soluble in the liquid phase of ether and therefore accumulated at the edge of the boiling zone as shown. The front was observed to remain roughly circular. This is in contrast to the earlier results of Fitzgerald, Pruess and van Rappard (1996) where tongues of liquid were observed to move rapidly and erratically through a smooth-walled fracture. It is believed that the smooth-walled fracture aperture used in the earlier boiling experiments may have increased with radius due to the deformation of the apparatus during heating. Furthermore, the flow rates used in the earlier boiling experiments were sufficiently high that inertial effects were likely to have been important. The present experimental results provide a much more reliable data set to test the numerical prediction of TOUGH2. The numerical problem considered for comparison with the experimental observations was a two-dimensional radial system with semi-infinite fracture walls as illustrated in Figure 1.4.

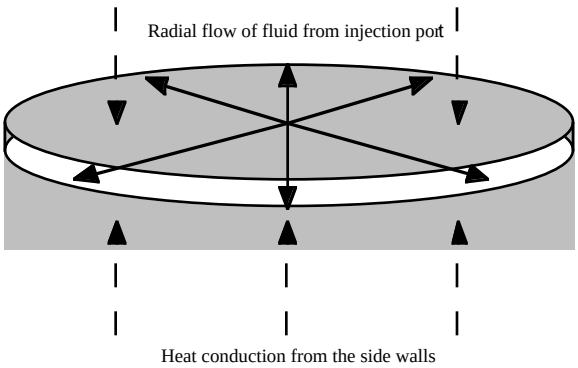

Figure 1.4 Schematic diagram illustrating the radial flow of fluid through the fracture apparatus and the conduction of heat within the glass walls bounding the fracture.

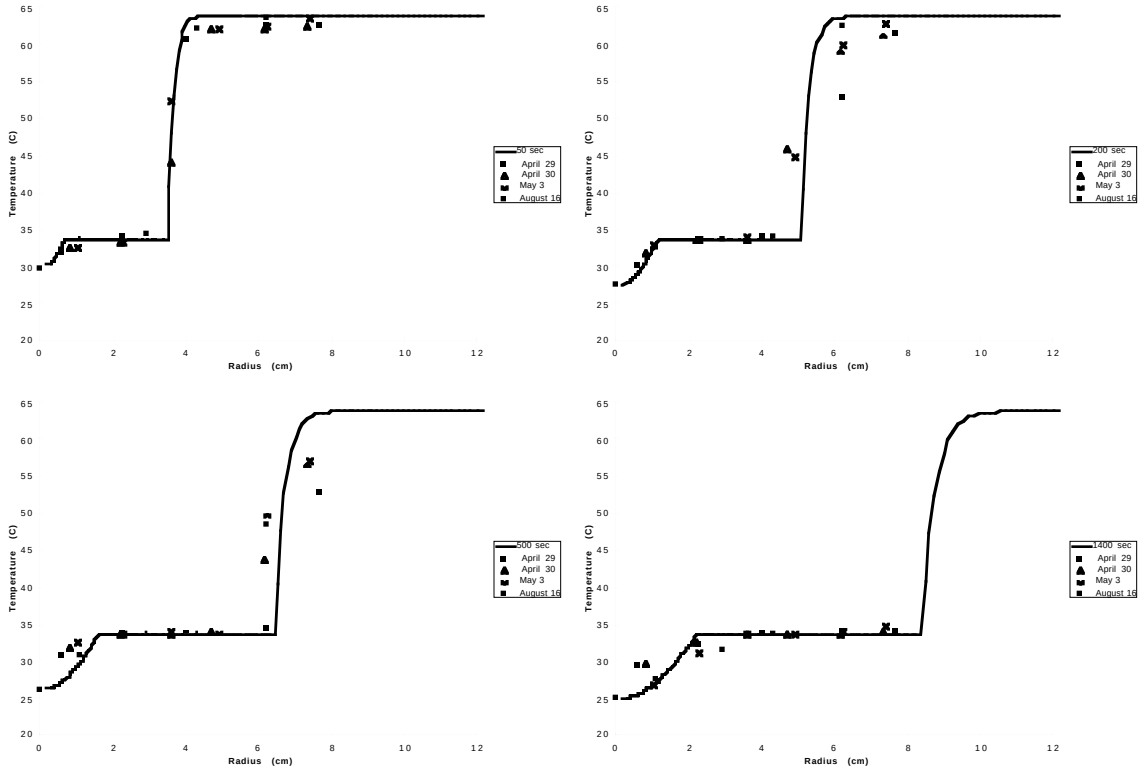

Figure 1.5 Temperature profiles at times 50, 200, 500 and 1400s after the onset of injection of 21°C liquid ether at 10 ml/min into a fracture originally at 64°C. The symbols represent data obtained from different experiments and the solid line indicates the profile obtained from the modified numerical code TOUGH2.

In order to compare the numerical prediction of the code with the experimental results, the code was modified to incorporate the physical properties of ether rather than water for the reservoir/apparatus fluid. For example, properties of ether at atmospheric conditions include: vapor density 3.331kg/m^3, liquid density 713.8kg/m^3, latent heat of vaporization 377.7kJ/kg, vapor viscosity 8.4e-6 kg/sm and liquid viscosity 1.66e-4 kg/sm

(Weast 1972). The problem of heat transfer from the brass injection port arose in the series of boiling experiments, as in the earlier non-boiling series. In order to compare the temperature profiles recorded at various stages in the experiment with the numerical prediction we placed a thermocouple within the fracture at the point of entry of the fluid.

As the experiment proceeded the inlet temperature of the liquid ether to the fracture decreased as expected. In order to account for this effect, the inlet temperature of the liquid used in the numerical fracture model was reduced at various times in accord with the experimental observations. Experiments were conducted at flow rates of 10 and 20 ml/min. Typical temperature profiles at various times for the two flow rates are shown in Figures 5 and 6.

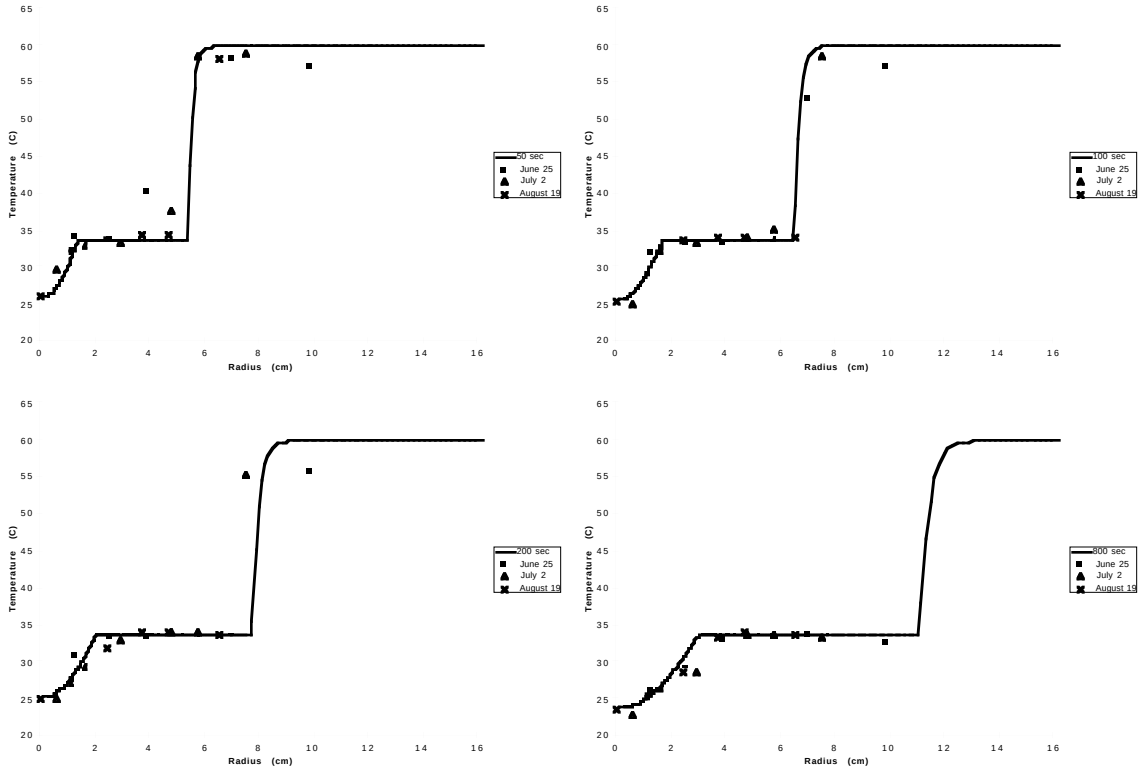

Figure 1.6 Temperature profiles at times 50, 100, 200 and 800s after the onset of injection of 21°C liquid ether at 20 ml/min into a fracture originally at 60°C. The symbols represent data obtained from different experiments and the solid line indicates the profile obtained from the modified numerical code TOUGH2.

It is seen that the agreement between the experimental observations and the numerical predictions is good. Close to the injection port a liquid-filled region develops as predicted. Within this liquid-filled zone the experimental data is in very close agreement with the numerical prediction. The radial temperature and temperature gradient increase away from the injection site until boiling conditions are attained. Ahead of the liquid zone lies a two-phase zone. The scatter of the experimental data becomes greater towards the leading edge of the two-phase zone. During the course of the experiments it was found that the leading edge of the boiling zone tended to pulse rather than migrate steadily. As a result, the

temperature may have fluctuated whereas the numerical prediction did not indicate this phenomena.

The average period of the pulses tended to increase as the two-phase region became larger. This pulsing may represent a form of instability at the interface between the two-phase region and zone of superheated vapor. Ahead of the two-phase zone the temperature was found to increase sharply across a thermal boundary layer to the far field temperature. The variations in experimental data were less marked further from the boiling zone due to the smaller influence of the pulses.

These experimental results suggest that the predictions for the evolution of the temperature, pressure and saturation distributions which one may obtain from TOUGH2 are likely to be very accurate for uniform horizontal fractures bounded by impermeable rock.

1.2.6 Conclusions

We have shown that the theoretical prediction for heat transfer at intermediate times in a fracture bounded by infinite rock is in good agreement with experimental observations. As liquid migrates out into the reservoir from an injection well feed point, the rock immediately surrounding the injection well is cooled rapidly. As the liquid migrates further into the fracture, the surface area of rock available for heating increases significantly. Eventually, the conduction of heat from the far field in the direction of fluid flow will become important and the theoretical expression discussed will break down.

In the case of liquid injection into a depleted reservoir, the migration of liquid along the fractures is much more complex. A liquid-filled region develops close to the injection well. A two-phase region develops ahead of this zone. Our experimental observations suggest that the injection and boiling of liquid in a fracture may be accurately described and modeled using existing numerical techniques (Pruess 1991). These results are extremely important since they represent the first laboratory experiments which have been conducted and confirm the validity of the numerical techniques for modeling injection and boiling in a fracture.

We are in the process of developing this work further by examining experimentally how an injection plume migrates under gravity and how the rate of propagation of the cold water changes when the rock bounding the fracture is permeable.

2 AN EXPERIMENTAL STUDY OF BOILING IN POROUS MEDIA

This research project is being conducted by Dr. Cengiz Satik. The objective of this study is to improve our understanding of the process of boiling in porous media by using both experimental and numerical methods.

2.1 SUMMARY

We report on a preliminary, horizontal boiling experiment conducted using a Berea sandstone core. The objective of this study is to improve the understanding of the process of boiling in porous media using both experimental and numerical tools. The ultimate goal is to determine the relative permeability and capillary pressure functions. In the last quarterly report, we presented the results of the first preliminary boiling experiment. The results of this first experiment indicated that further improvements on both the design of the core holder and the experimental technique were needed. During the last quarter, another core was manufactured and a boiling experiment was conducted. The results will be discussed here.

2.2 RESULTS AND DISCUSSION

The processes of vaporization and condensation in porous media are of significance in geothermal systems as well as in many other processes such as boiling in porous media, porous heat pipes, drying and nuclear waste disposal. Previous fundamental studies focusing at the microscopic pore scale have been very limited. In a recent study by Satik and Yortsos (1996), numerical and experimental pore networks were used to model boiling in porous media. Satik and Yortsos (1996) developed a numerical pore network model for boiling in a horizontal, two-dimensional porous medium and conducted visualization experiments by using glass micromodels. Although significant progress was made, their model was developed for a single bubble growth problem, ignoring effects of gravity. Therefore, further work is still needed to resolve the issues raised by the continuum formulations (see Satik 1994 for details) and to obtain correct forms of relative permeability and capillary pressure functions. In this project, we are adopting a different technique to study this problem. We are conducting boiling experiments with real core samples such as Berea sandstone and using an X-ray tomography (CT scanner) equipment to determine the fluid distributions within the core during the experiment. Our ultimate goal is to be able to carry out these experiments with core samples taken from The Geysers geothermal field in California. Concurrent efforts are also directed towards the construction of apparatus that can be used to carry out boiling experiments with tight core samples.

Details of the experimental apparatus and method for the boiling experiment were discussed in the previous quarterly report. Briefly, the apparatus consists of a core holder, a pressure measurement system, a temperature measurement system, a liquid pump and a balance. Several pressure taps, thermocouples and heat flux sensors are attached along the core length to measure pressures, temperatures and heat losses, respectively. To reduce the heat losses, the core holder is covered with a 2 inch thick insulation material. Finally, a

heater and a heat flux sensor are placed at one end of the core to impose and measure heat flux. During an experiment, the core holder is placed inside the high resolution X-ray CT equipment in order to obtain *in-situ* saturation profiles along the core. Principles of X-ray CT usage in porous medium flow experiments are described elsewhere (Johns *et al.* 1993). Before starting an experiment, air inside the pore space is removed. The core is then scanned at predetermined locations to obtain dry-core CT values. Next, water is injected into the core to saturate it with water completely, at which time the core is X-ray scanned again at the same locations to obtain wet-core CT values. Pressure readings are taken at this time to calculate absolute permeability while three-dimensional porosity distributions are obtained by using these two sets of CT data. Steady-state boiling experiments mainly involve injection of heat into the core at varying power values. During the experiment, the heating end of the core is closed to fluid flow while the other end is connected to a container placed on a balance, which is used to monitor the amount of water coming out of the core during the experiment. Continuous measurements of pressure and temperature are taken during each heat injection rate step until steady state conditions are reached. During the boiling process each step continues until the water production rate becomes zero, and the pressures and temperatures stabilize; these are indications of steady-state conditions. At the onset of steady-state conditions, the core is scanned again at the same locations to obtain CT values corresponding to the particular heat flux value. To complete the set of measurements, pressure, temperature and heat flux readings are recorded again. The heat flux is then changed, and the procedure is repeated. Using the three sets of CT data, three-dimensional saturation distributions are calculated (Satik *et al*., 1995). Starting from a completely water saturated core and increasing the heat flux value gives rise to a boiling (drainage) process while the opposite procedure leads to condensation (imbibition).

During the last quarter, a horizontal boiling experiment was conducted. The core used in this experiment was a Berea sandstone, the length and diameter of which were 40.6 cm and 5.04 cm, respectively. We obtained a complete set of experimental data for the case in which the heat flux was increased, which included porosity and saturation distributions determined using the X-ray CT data, and also pressure and temperature readings.

As described in the last quarterly report, we obtained rather unusual results from the first preliminary experiment. The comparison of the steam saturation profiles obtained from the X-ray CT scanning with the corresponding temperature and pressure profiles indicated an inconsistency. The steam saturation profiles showed non-zero steam saturation at temperatures of as low as 50 ^{o}C at pressures above atmospheric pressure. This was initially attributed to air possibly trapped inside porous medium and also to air dissolved in the water used to saturate the porous medium. To remedy this problem, the experimental procedure was changed to remove any possible initial gas phase existing in the system. During the new procedure, the core was first vacuumed to $165*10^{-3}$ torr before the experiment. The water used to saturate the core was then deaerated by boiling it in a container. The core was X-ray CT scanned eight times to observe the formation of the first steam phase. In Figure 2.1, we show the average porosity profiles along the core, obtained from the X-ray CT scanning conducted at three different times before the heating and at five different times after the heating . In all of the figures given in this section, t and

HF represent the time elapsed and heat flux values used during the experiment, respectively. Each of these porosity values shown in the figure were calculated by averaging the porosities at each circular cross-section of the core that was scanned. All of the curves in the figure, except the curve at time= 2830 min. and heat flux= 7750 W/m^2, show a fairly uniform porosity profile along the core. The average porosity of the whole core was calculated to be around 20%. The curve corresponding to time= 2830 min. and heat flux= 7750 W/m^2 in Figure 2.1 shows a deviation at distances closer to the heater which suggests the first appearance of the steam phase. Since a comparison of the curves in Figure 2.1 with pressure and temperature data indicated that a steam phase did not appear until the appropriate boiling temperature, this confirms air was successfully removed from both porous medium and the water used to saturate it.

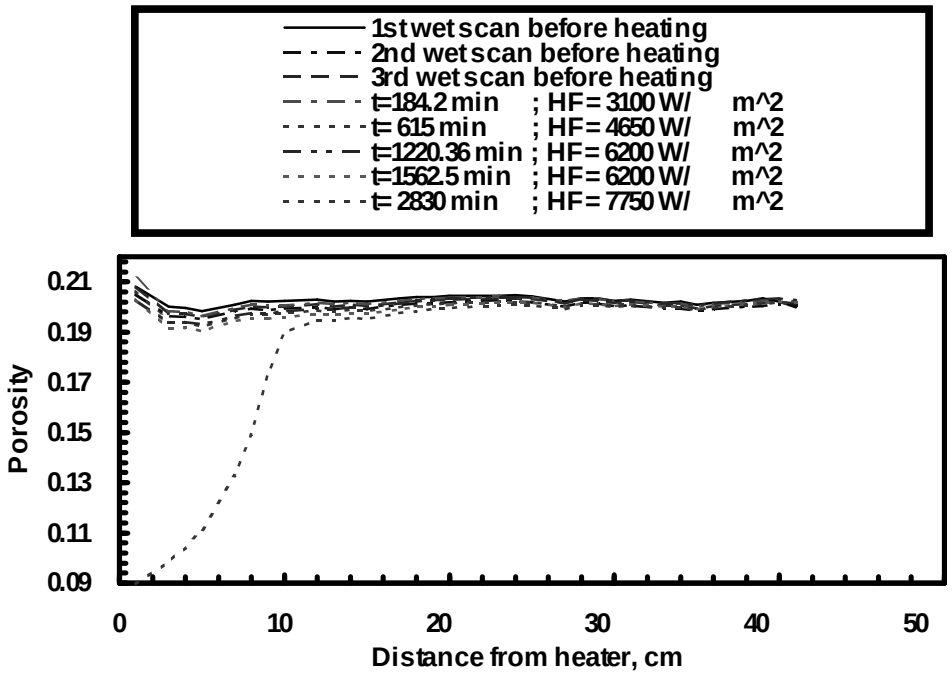

Figure 2.1 Average porosity profiles along the core, obtained from the X-ray CT scanning conducted at three different times before the heating and at five different times after the heating.

The boiling experiment was conducted by increasing the heater power value incrementally to reach a desired heat flux value. The heat flux values corresponding to the power values used were calculated to be 6200, 7750, 9300 and 10850 W/m^2, respectively. These are large heat flux values compared to the heat flux values typically observed in geothermal systems (~0.5 W/m^2). In Figure 2.2, we show the heat flux values used during the experiment, calculated from the heater power settings.

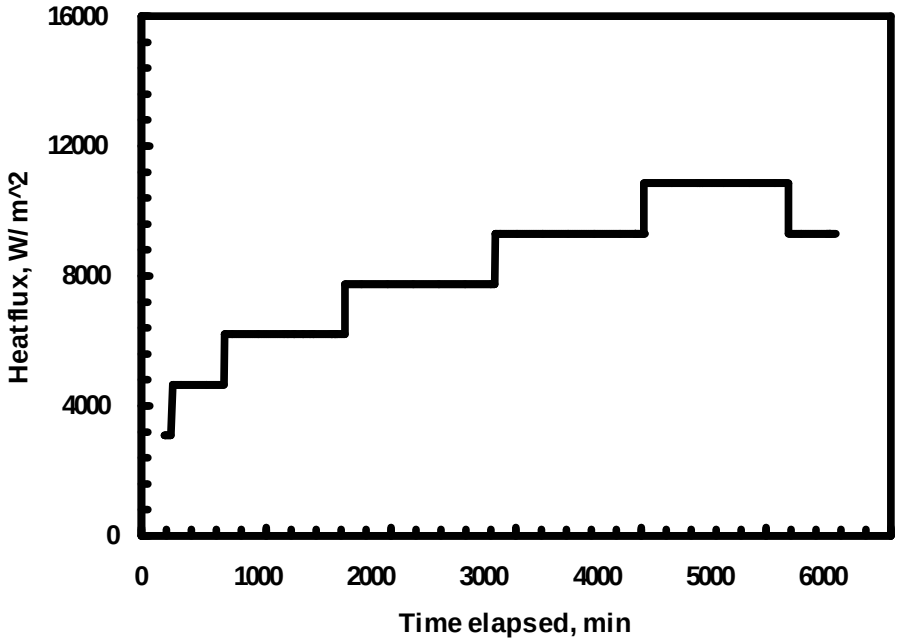

Figure 2.2 Heat flux values obtained from the heater power settings.

In the last quarterly report, we showed that the heat flux values from the sensor readings are about 35% of those from the heater power settings. This meant that only 35% of the total heat flux generated by the heater was in the axial direction since the heat flux sensor measured the axial heat flux. To reduce the heat losses from the heater and to direct most of the heat flow in the axial direction, an improved design of the heating section of the core holder was employed during this experiment. However, we believe that further improvements are needed since a substantial amount of heat produced by the heater is still transferred radially and from the other side of the heater.

During the experiment, we recorded both the centerline and wall temperatures at various locations along the core. In Figure 2.3, we show the centerline temperature histories obtained at the 11 locations. These temperatures were measured along the centerline of the core. The figure shows both transient and steady state (where the temperature profile flattens) sections of the temperature profiles at each heat flux value. The maximum temperature reached during this experiment was 225^{o}C. A comparison of the four centerline and wall temperatures are shown in Figure 2.4. The wall temperatures were measured over the outer layer of the epoxy. As shown in Figure 2.4, the maximum difference between the two temperature profiles is less than 1 ^{o}C. This suggests that the radial temperature gradient along the core was not significant for this set of experimental conditions (i.e. core diameter of 5.08 cm) and therefore it would be adequate to measure wall temperatures only.

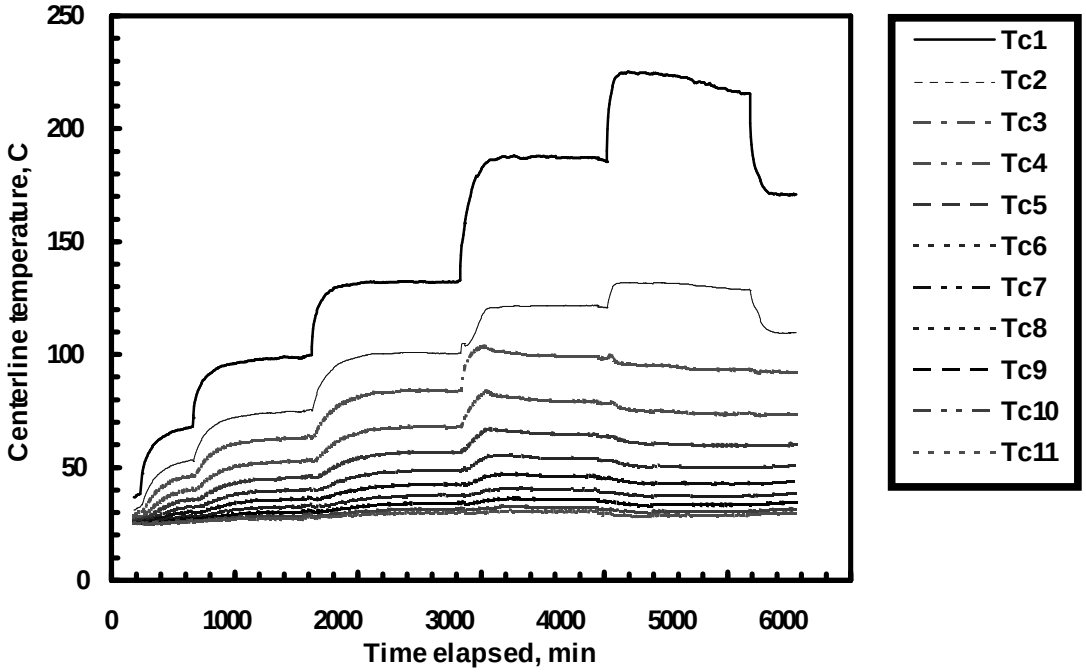

Figure 2.3 Temperature history obtained from the eleven thermocouples located along the core length.

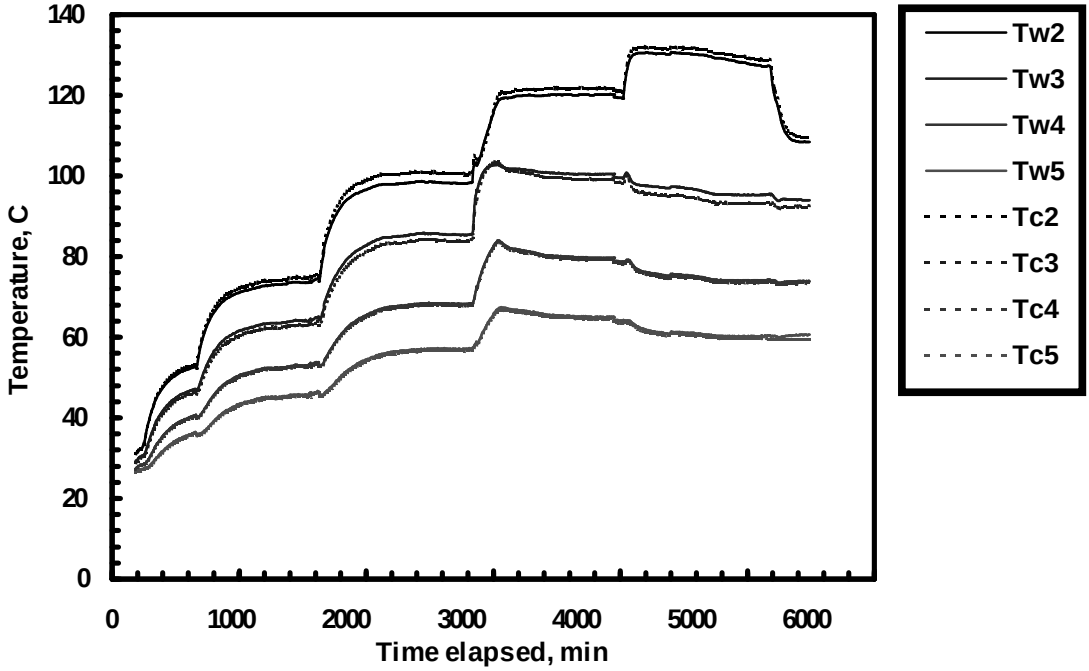

Figure 2.4 Comparison of four centerline and wall temperatures.

In Figure 2.5, we show the steady state, average steam saturation profiles at the four heat flux values, calculated from the X-ray CT data. The saturation profile at t=2830 min and HF= 7750 W/m^2 shows a two-phase (steam and water) zone followed by a completely water-filled zone while the profile at t= 3970 min and HF= 9300 W/m^2 shows three distinct regions of completely steam, two-phase and completely water. The steam saturation is higher at locations closer to the inlet, where the heater is located, and decreases towards the outlet. A comparison of these saturation profiles with the centerline temperature profiles given in Figure 2.6 shows that the previous problem of the apparent existence of a gas phase at inappropriate temperatures still exists. More efforts will be given during the next quarter to understand and to resolve this problem. Concurrent efforts will also be given in the numerical direction to compare the experimental findings with the results of a numerical simulator (i.e. TETRAD). In addition, we plan to run the simulator in combination with an optimization routine to infer relative permeability functions for the problem of boiling in porous media.

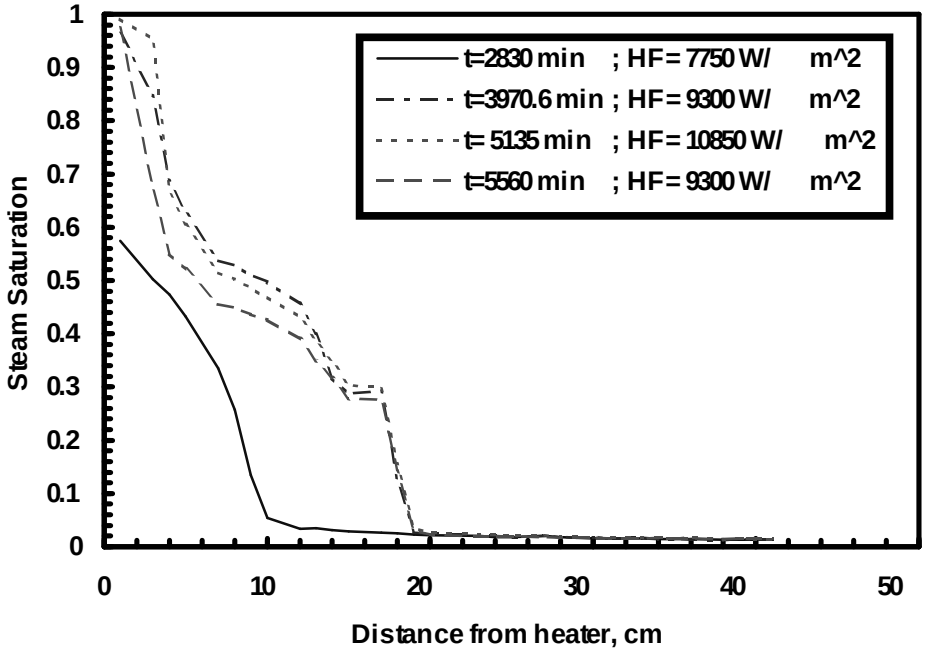

Figure 2.5 Steady state steam saturation profiles along the core, obtained from X-ray CT data.

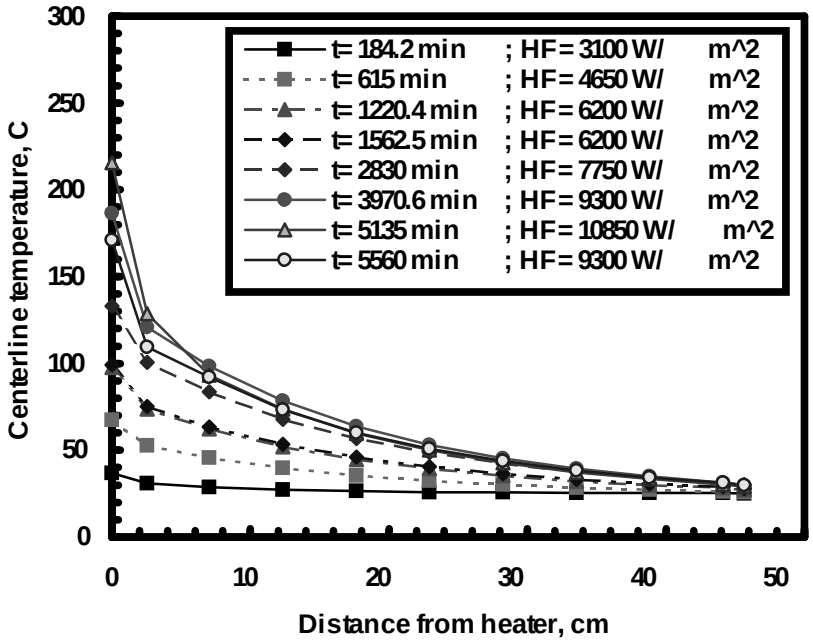

Figure 2.6 Steady state, centerline temperature profiles along the core.

3 STEAM-WATER RELATIVE PERMEABILITY MEASUREMENT

This project was conducted by Research Assistant Raul Tovar, Dr. Cengiz Satik and Professor Roland Horne. The aim of this project was to measure experimentally relative permeability relations for steam and water flowing simultaneously in a porous medium.

3.1 SUMMARY

As discussed in the previous report, a set of relative permeability relations for simultaneous flow of steam and water in porous media have been measured in a steady state experiment conducted under the conditions that eliminate most errors associated with saturation and pressure measurements. These relations showed that the relative permeabilities for steam-water flow in porous media vary approximately linearly with saturation (Ambusso 1996). This departure from the nitrogen/water behavior indicates that there are fundamental differences between steam/water and nitrogen/water flows. Since then, improvements for the acquisition of experimental data have been made so that all experimental data is collected by and analyzed in a personal computer. However, while attempting to measure steam-water relative permeability using this new data acquisition equipment, experiments failed three times as a result of high pressure differentials close to inlet, which later caused excessive leaks. These will be discussed in this section.

3.2 INTRODUCTION

The concept of relative permeability is an attempt to extend Darcy's law for single-phase flow of a fluid through porous media to account for simultaneous flow of several phases. In this regime the flow of each phase is governed by the microscopic pressure gradient of each phase and the fraction of the overall permeability that is associated with it. This fraction, normally expressed as a fraction of the medium's permeability to single-phase fluid, is called the relative permeability. Since being introduced by Buckingham in 1907 and used extensively by investigators in the 1930's, relative permeability has been traditionally expressed as a function of saturation principally because it was believed that it depended on the pore volume occupied by the fluids (Hassler 1944). In addition it is necessary to define residual saturations which normally indicate the smallest saturation for a given phase to become mobile. The curves and the residual saturations together define the relative permeability relations. For most cases these relations can be expressed as simple mathematical functions (Corey 1954; Brooks and Corey 1964). Application of Darcy's law to the description of simultaneous flow of two or more phases of fluids in a porous medium requires the use of relative permeability relations (Hassler 1944; Osoba *et al.* 1951; Corey 1954; Brooks and Corey 1964). In most applications in petroleum engineering such as those involving the flow of oil and water as in water flooding, and oil and gas as in gas injection, these relations are well known and can be determined from routine laboratory experiments (Osoba *et al.* 1951). However, for the flow of steam and water or for the general case of single-component two-phase flows, these relations are not well known. To our knowledge, none of the relations that have been reported in the last few decades are known to be completely error free (Verma 1986; Sanchez 1987). The

main sources of error in these experiments, as we show later in this report, were due to inaccurate measurements of fluid saturations and inappropriate assignment of pressure gradients to individual phases.

Other techniques involving analysis of enthalpy transients from producing geothermal fields have been used to infer relative permeability relations (Grant 1977; Sorey *et al.* 1980; Horne and Ramey 1978). However these techniques do not eliminate all the variables and quite often the *in-situ* fluid saturations and the overall permeability structure (i.e matrix, fracture) are unknown. Therefore, these curves are approximations at best. As shown by the experiments reported by Osoba *et al.* (1951) and by Hassler (1944), laboratory measurements of relative permeability can still be prone to significant errors if capillary end-effects are not taken into account. The end-effects are known to cause pressure gradients, and by extension, saturation gradients resulting in a nonuniform distribution of fluids in the core particularly at low flow rates. Ignoring this effect may result in an underestimation of the relative permeability of the wetting phase and the attribution of a permeability value for the nonwetting phase to an erroneous value of saturation (Verma 1986).

3.4 EXPERIMENTAL APPARATUS

The description of the apparatus for these experiments was discussed in Satik *et al.* (1995) and Ambusso (1996) and is shown in Figure 3.1. In general, it consists of an injection unit and a core holder made of epoxy. The injection unit consists of two furnaces to generate steam and hot water. Two temperature controllers are used to control the temperatures of the two furnaces. Heat losses on the core body are measured by using eight heat flux sensors. Temperatures are measured by seventeen thermocouples. Nine J-type thermocouples are placed along the steam injection, water injection and outlet lines. Eight T-type thermocouples and the eight heat flux sensors are placed at equal intervals along the core body. Pressures are measured by using seventeen pressure transducers. All of the experimental data is collected and analyzed by a data acquisition system. The proportional voltage signals from the heat flux sensors, thermocouples and pressure transducers were first conditioned by the data acquisition system and then they were collected and analyzed in a personal computer using "LABVIEW", a graphical programming software. "LABVIEW" uses a control panel as an interactive interface for observing outputs from the experimental apparatus. It uses a code diagram that contains icons representing input/output operations, computational functions, and analysis functions to organize the program source code. The source code is a modification of a "temperature monitor" program included in the software package. It monitors temperatures, heat fluxes and pressures on four charts as well as on digital indicators. The user has the option to save the data in spreadsheet form as often as needed, allowing further data processing and analysis. Modifications made over the last quarter included the use of a steam table data base to alert the user if saturation conditions have been reached, crucial to the control of the experiment. In addition it calculates real time flowing fractions of steam and steam-water relative permeability as outlined below.

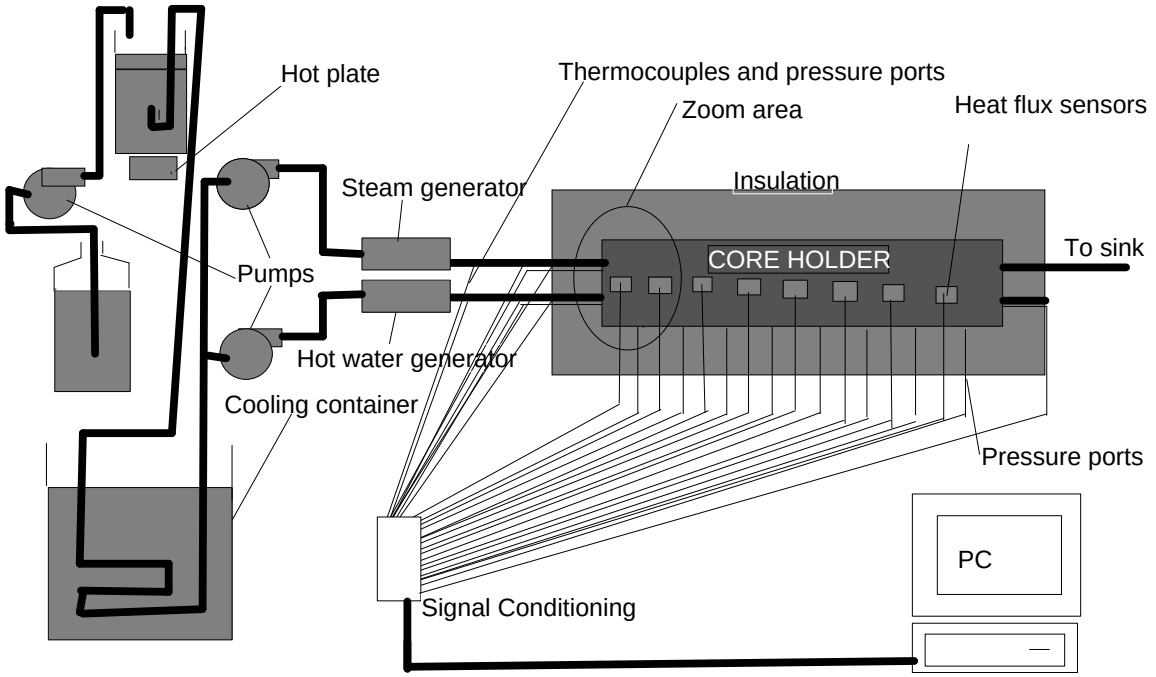

Figure 3.1 Experimental Apparatus.

and thermocouples

The core (rock) samples used for these experiments have been described in detail by Ambusso (1996) and had the following properties; type of Berea sandstone, permeability of 600 md, porosity of 20%, length of 38 cm and diameter of 5.04 cm. A core sample is first heated to 450 ^{o}C for twelve hours to deactivate clays and to get rid of residual water. Eight ports to measure temperatures and pressures are then fitted at fixed intervals along the edge of the core before the rest of the core is covered completely by high temperature epoxy. The core is tested for leaks before being covered with an insulation material made of ceramic blanket. During an experiment saturations are measured by using a high resolution X-ray CT scanner. Relative permeabilities are then calculated using the pressure and temperature data and the equations derived in the following section.

Note from Figure 3.1 that in the new arrangement mixing of the steam and water fluids takes place inside the core. This injection system was modified in order to avoid calculation errors. Heat losses in the injection lines were previously calculated from an empirical correlation at sub-cooled conditions which does not account for the drastic change of the heat transfer coefficient of the fluid as it reaches saturated conditions. In the future, air trapped in the water that could give erroneous saturation readings, will be removed by boiling it and then cooling it before injecting it into the core as shown in Figure 3.1. Also, the core will be vacuumed to remove the air inside it using a vacuum pump instead of displacing it by flowing CO_2.

3.5 CALCULATIONS

Mass flowing fractions can be calculated by applying the following mass and energy conservation equations:

$$m_t = m_v + m_l \tag{3.1}$$

$$m_v h_v + m_l h_l = m_t h_t + Q \tag{3.2}$$

where m and h refer to mass flow rate and enthalpy, respectively and the subscript *t* refers to total, *v* to vapor phase and *l* to the liquid phase. *Q* is the total heat lost upstream of the point being considered.

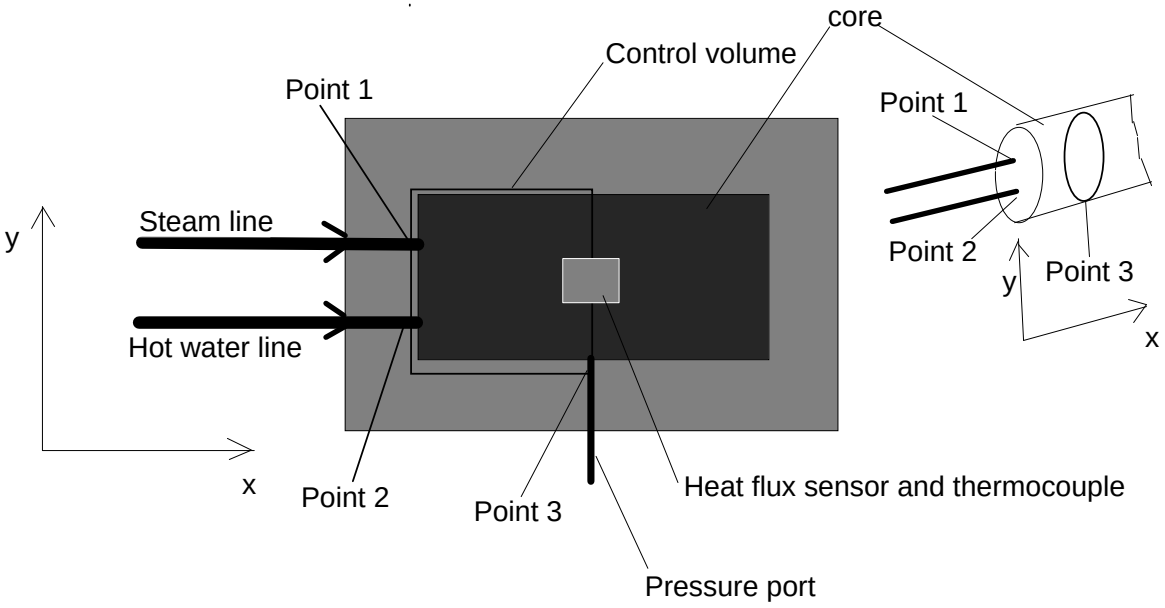

Figure 3.2 Control Volume From Figure 3.1 Zoom Area.

To apply the equations to the control volume in Figure 3.2 we will inject at point 1 superheated steam at a known rate m_1, pressure p_1 and temperature T_1. At the same time we will inject sub-cooled water at point 2 at a known rate m_2, pressure p_2 and temperature T_2. From T_1 and p_1 using superheated steam tables we can interpolate to obtain h_{1v}. From T_2 and using saturated steam tables we can approximate h_2 by using h_{2l}, the enthalpy at the saturated liquid phase. At point 3, when saturation is reached, either from p_3 or T_3 using saturated steam tables we can obtain h_{3l} and h_{3lv}, the liquid phase enthalpy and the latent heat of vaporization respectively. *Q* is obtained by using *Q", the* heat flux sensor value:

$$Q = Q'' A \tag{3.3}$$

where *A* is the surface area of the core from either point 1 or 2 to point 3.

Thus Equation (3.1) becomes:

$$m_3 = m_1 + m_2 \tag{3.4}$$

and (3.2) becomes:

$$m_1 h_{1v} + m_2 h_{2l} = m_3 h_3 + Q'' A \tag{3.5}$$

where:

$$h_3 = h_{3l} + x h_{3lv} \tag{3.6}$$

Thus the steam fraction x in the flow at any time can be calculated by

$$x = \frac{m_1 h_{1v} + m_2 h_{2l} - Q'' A}{m_3 h_{3lv}} - \frac{h_{3l}}{h_{3lv}} \tag{3.7}$$

Then the relative permeabilities to steam and water can be calculated by the corresponding Darcy equations for each phase in terms of the mass flow rates

$$k_{rl} = -\frac{(1-x) m_t \mu_l \nu_l}{kA \dfrac{\Delta p}{\Delta x}} \tag{3.8}$$

and

$$k_{rs} = -\frac{x m_t \mu_s \nu_s}{kA \dfrac{\Delta p}{\Delta x}} \tag{3.9}$$

Thus, a knowledge of the values of flowing mass fractions in the above equations and pressure drop along a column of the core with constant or flat saturation provides a value for the relative permeability.

Q, calculated kW	**T_1** C	**h_1** KJ/Kg	**m_1** Kg	**T_2** C	**h_2** kJ/Kg	**m_2** Kg	**T_3** C	**h_3** kJ/Kg	**m_3** Kg
0.00158858	40.0	168	8.33E-05	36.0	151	8.33E-05	35.8	150	1.67E-04

Q, measured kW	**Q"** KW/m^2	**A** m^2
0.00153216	1.92E-01	7.98E-03

Table 3.1 Heat loss calculation.

In order to verify the validity of Equation (3.5) for heat losses Q, we have used experimental data at sub-cooled conditions to calculate it as shown in Table 3.1. Sub-cooled conditions are necessary for the verification since the enthalpies are known. Thus Q "calculated" was obtained by solving Equation (3.2). Q "measured" was obtained using Equation (3.3). Table 3.1 shows that they are in good agreement as expected with a percentage difference of about 3.27%.

3.6 CONCLUSION

Several relative permeability relations for flow of steam and water in porous media derived from experiments have been proposed in the past (Chen *et al.* 1978; Council and Ramey 1979; Verma 1986). In all of the curves reported in the past the relative permeability for one or more of the phases have tended to follow the relations obtained by Corey (1954) for nitrogen and water. However, none of the previous investigations involved the use of the experimental apparatus described here, which includes significant improvements in measuring saturation, temperature and pressures. In the last quarterly report, we presented a preliminary set of steam/water relative permeability relations.

During the current quarter, we have improved our experimental apparatus by using a better data acquisition system as well as modifying the core injection, a possible source of error. With such improvements, we hope to repeat the previously reported measurements of steam-water relative permeability during the next quarter in order to confirm or improve the results. Further measurements at different temperatures, flow rate, absolute permeability, and orientation (e.g. vertical instead of horizontal) will also be investigated. We will attempt to repeat the steam-water relative permeability experiments with the improved apparatus.

4 HEAT PIPES

This project is being conducted by Program Manager Prof. Shaun D. Fitzgerald, Research Assistant Noel Urmeneta. We are also collaborating with Prof. Andrew W. Woods at the University of Bristol. In this study we are investigating convective heat transfer within a heat pipe. We are seeking to extend our current understanding, which is primarily based on the case of porous medium type heat pipes, to the situation where a reservoir is fractured. During the last three months, we have made considerable progress in the development of a model for determining the stability of two-phase heat pipes. The earlier model which had been developed was based upon the assumption that the quasi-steady heat flux within a two-phase zone (Bau and Torrance 1982) could be used in a perturbation expansion in order to derive a dispersion relationship. This is not strictly permissible, and we have therefore developed a simple model which we first describe below. We then discuss the numerical work performed during the last 3 months on the two-dimensional model of a heat pipe system.

4.1 STABILITY OF HEAT PIPES

This project is being conducted by Program Manager Prof. Shaun D. Fitzgerald in collaboration with Prof. Andrew W. Woods at the University of Bristol, Prof. Kent Udell at the University of California Berkeley and Undergraduate Research Assistant Catherine Tsui-Ling Wang.

4.1.2 Introduction

Vapor-dominated geothermal reservoirs, including the Geysers, California, consist of a vapor-dominated two-phase zone, 1000-3000m deep (White, Muffler and Truesdell 1971; Schubert and Straus 1980; Truesdell and White 1973), overlain by a single phase liquid zone, 0.3-1km deep. Since two-phase zones are highly compressible it is puzzling as to why the dense overlying liquid does not sink into the two-phase zone or conversely why the two-phase zone does not drive out the liquid to form a two-phase boiling zone which extends to the surface, as in the hot spring/geysers areas at Wairakei, New Zealand and Yellowstone, USA (Grant, Donaldson and Bixley 1982; White *et al*. 1975). Here we show that if there is a region of relatively low porosity, <0.1-1.0%, at the interface between the liquid and two-phase zones, then the interface may be stable. Our model is consistent with field evidence from the Geysers, in which a low-porosity shale divides the liquid and two-phase zones (Ramey 1970), and it suggests why such geothermal systems are relatively rare.

4.1.2 Theoretical Model

Understanding the physical state of geothermal and hydrothermal systems is crucial for geothermal power generation (Muffler and Truesdell 1971; Schubert and Straus 1980; Truesdell and White 1973; Grant, Donaldson and Bixley 1982; White *et al*. 1975; Ramey 1970; Elder 1981) and hazard analysis at volcanic crater lakes (Brown *et al*. 1989;

Christenson and Woods 1991). In geothermal systems such as the Geysers, California and Larderello, Italy, heat is conducted through the upper liquid-saturated part of the system along a temperature gradient as large as 1°C/m (Ramey 1970). Below this there is a vapor-dominated zone, in which the temperature follows the boiling point with depth for saturated vapor, suggesting that there is some liquid in contact with the vapor but that the pressure is controlled by the vapor phase (Figure 4.1*a*). The temperature gradient is much smaller in this zone (Figure 4.1*a*), and therefore, in order to match the large conductive heat flux through the overlying liquid zone, it is thought that heat is transported upwards through the vapor-dominated zone by the heat-pipe process (Truesdell and White 1973; Grant, Donaldson and Bixley 1982; Ramey 1970; Ingebritsen and Sorey 1988): high enthalpy vapor ascends and condenses at the top of the layer while an equal mass flux of low enthalpy liquid descends and boils at the base of the layer.

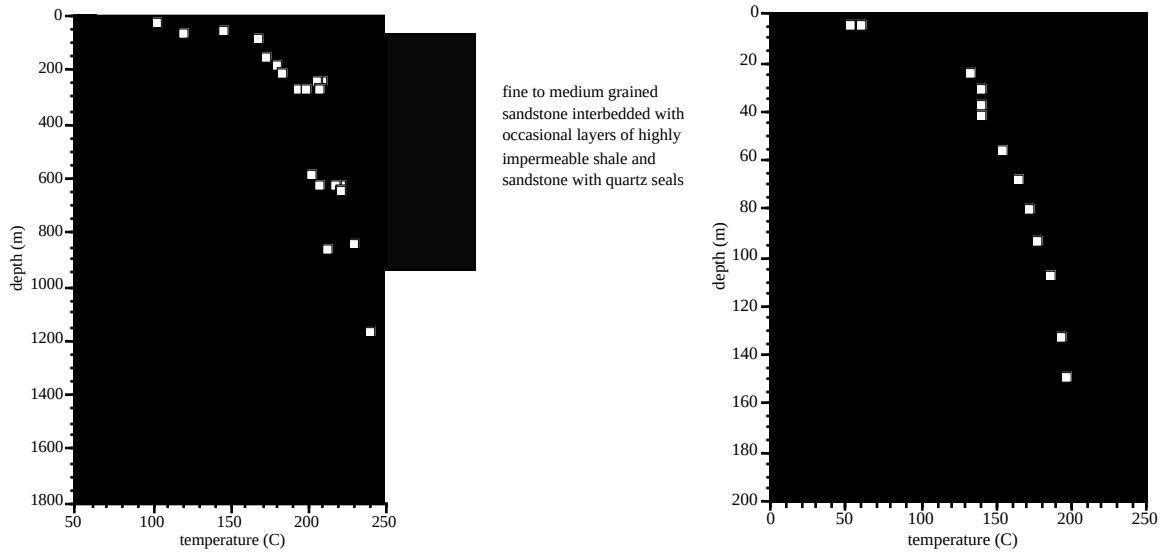

(*a*) (*b*)

Figure 4.1 Temperature and saturation temperature profiles at (a) the Sulfur Bank-Happy Jack area of The Geysers reservoir California after the data of Ramey (1970) and open file well logs (California Div. Oil & Gas); squares indicate temperature measurements, circles represent saturation temperatures corresponding to pressure measurements, the solid line indicates a region of vertical heat transfer by conduction, the hatched line indicates a region of vertical heat transfer by a vapor-dominated convective heat pipe, (b) in well Y-3 at Yellowstone taken from White et al. (1975) squares indicate temperature measurements, the dashed line represents the temperature profile corresponding to a column of boiling liquid (boiling point for depth profile).

Given this picture, it is intriguing how such a system is stable since the overlying cool liquid is much denser than the two-phase mixture and furthermore the two-phase mixture is very compressible. Schubert, Straus and Grant (1980) examined the stability of a liquid-over-vapor system to the fingering instability, assuming the vapor to be incompressible. Their analysis showed that the interface is stable if the background heat flux is sufficient to vaporize descending fingers of liquid. Since the fingers descend at a speed $K\Delta\rho g/\mu$,

where $\Delta\rho$ is the density contrast between the liquid and vapor, K is the permeability and μ the liquid viscosity, they will be vaporized if $Q>L\rho K\Delta\rho g/\mu$ where Q is the background heat flux (Schubert, Straus and Grant 1980; Woods and Fitzgerald 1996). This result also applies for the case of liquid overlying a two-phase zone (Woods and Fitzgerald 1996): typically, for such a geothermal system, $Q\approx 1\mathrm{W/m^2}$, and so for finger-stability, the permeability near the interface between the liquid and two-phase zone $K<10^{-17}\mathrm{m^2}$ (Schubert, Straus and Grant 1980; Woods and Fitzgerald 1996).

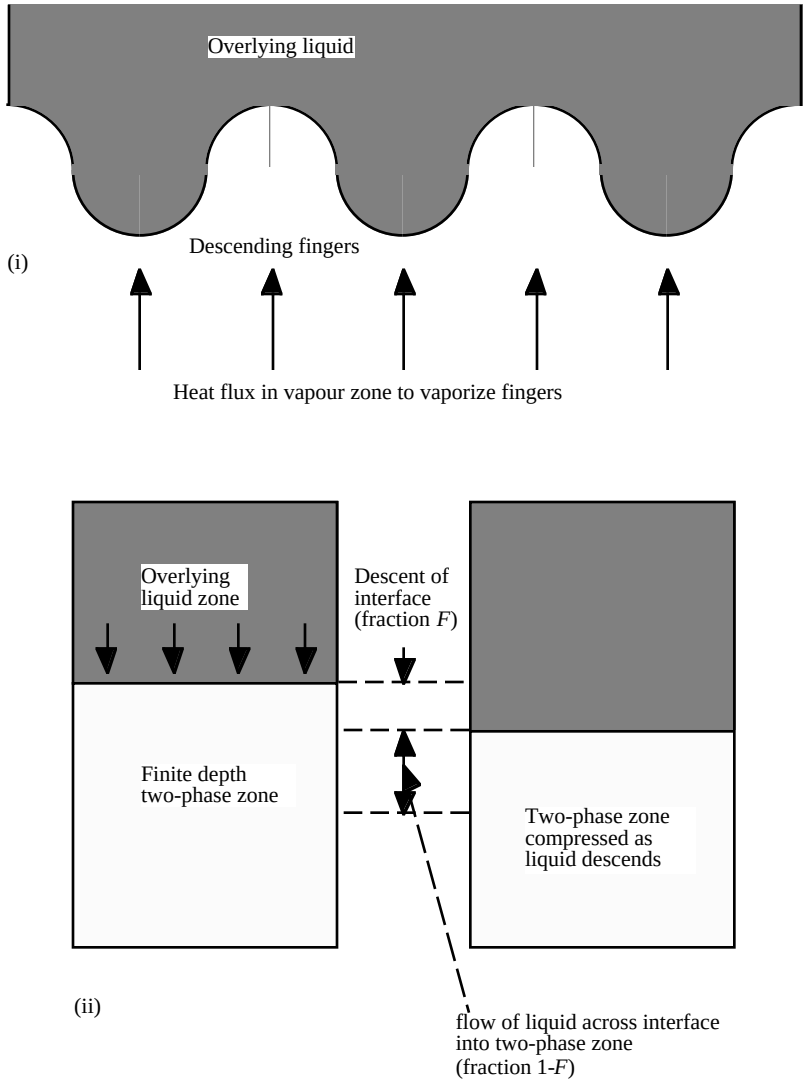

Figure 4.2 Schematic of a layer of liquid descending into a two-phase zone, identifying (i) the fingering style of instability (Schubert, Straus and Grant 1980) and (ii) the direct compressional mode described herein.

However, a fundamentally different and previously unrecognized type of instability may arise owing to the compressibility of the two-phase zone. We examine this herein. Essentially, when a depth δh of liquid descends into a vapor-dominated zone of finite volume, the hydrostatic pressure of the liquid overlying the two-phase zone increases. If

this exceeds the increase in the pressure of the two-phase zone which results from the compression, then the system is unstable (Figure 4.2). The change of pressure of the two-phase zone is given by

$$\partial P_{\mathrm{v}} = \frac{\partial h}{h\beta} \tag{4.1}$$

where h is the depth of the two-phase zone and β the compressibility. If the overlying layer of water is connected to a shallow aquifer, then the upper surface of the water table will not change appreciably as a result of the displacement. Therefore, the change in hydrostatic pressure acting on the two-phase zone, δP, depends on the density difference between the two-phase zone and the liquid, $\Delta\rho$, and also on the fraction F of the descending liquid which reaches the boiling temperature and becomes incorporated into the two-phase zone (Figure 4.2)

$$\partial P_{\mathrm{g}} = \Delta\rho g(1-F)\partial h \tag{4.2}$$

For a vapor-dominated two-phase zone, $\Delta\rho \approx \rho_{\mathrm{l}}$, the liquid density, since the vapor density is much smaller than that of the liquid.

Comparing (4.1) and (4.2) we deduce that the system is unstable whenever the depth of the liquid layer

$$h > h_{\mathrm{c}} = \frac{1}{\Delta\rho g\beta(1-F)} \tag{4.3}$$

The maximum depth of a two-phase zone which can be stably overlain by a layer of liquid, h_{c}, therefore depends on (i) F, the fraction of the descending liquid which is heated to the boiling temperature and becomes incorporated into the two-phase zone; and (ii) β, the compressibility of the two-phase zone.

F may be found by noting that in a porous layer, isotherms migrate with speed (Bodvarsson 1972)

$$u_{\mathrm{T}} = \frac{\rho_{\mathrm{l}} C_{\mathrm{pl}}}{\phi_{\mathrm{i}}\rho_{\mathrm{l}} C_{\mathrm{pl}} + (1-\phi_{\mathrm{i}})\rho_{\mathrm{r}} C_{\mathrm{pr}}} u \tag{4.4}$$

where u is the Darcy velocity, ϕ_{i} is the porosity of the matrix at the interface and C_{pl}, C_{pr} and ρ_{l}, ρ_{r} are the specific heats and densities of the liquid, l, and rock matrix, r. In contrast, the liquid itself only moves through the pore-spaces and therefore advances at a speed u/ϕ_{i} (Figure 4.2). Thus, as liquid descends along the uniform temperature gradient just above the interface, the fraction of the liquid heated to the boiling temperature is (Woods and Fitzgerald 1996)

$$F = 1 - \frac{\rho_{\mathrm{l}} C_{\mathrm{pl}}}{\phi_{\mathrm{i}}\rho_{\mathrm{l}} C_{\mathrm{pl}} + (1-\phi_{\mathrm{i}})\rho_{\mathrm{r}} C_{\mathrm{pr}}} \tag{4.5}$$

This relation reveals the important result that $1-F \ll 1$ in regions of very low porosity, essentially because there is a very large relative mass of matrix available to heat up the liquid.

The compressibility β may be found by noting that when a two-phase zone is compressed, there is a small change in the saturation temperature, leading to condensation of some of the vapor and a decrease in the volume. Grant and Sorey (1978) have shown that as a result, the compressibility of the two-phase zone has the approximate form

$$\beta = \frac{(1-\phi_i)\rho_r C_{pr} + \phi S \rho_l C_{pl}}{\phi L (dP_c/dT)\rho_v} \tag{4.6}$$

where ϕ denotes the mean porosity of the two-phase region, $P_c(T)$ is the saturation pressure as a function of temperature T, L is the heat of vaporization. Note that for $\phi<0.1$, β depends only weakly on S, the volume fraction of the void space occupied by liquid.

Combining equations (4.3-4.6), we can calculate the maximum depth of a two-phase zone which may be overlain by liquid. Figure 4.3 shows how this depth varies with the porosity near the interface between the liquid and two-phase zone. Curves are shown for interface porosities of 8, 1 and 0.5% with the mean porosity of the two-phase zone fixed at the typical value of 8% (Pruess and Narasimhan 1982). It is seen that an extensive two-phase zone, >1km deep, can only exist in a quasi-steady state if the porosity near the interface is sufficiently small, $\phi_i<0.5$-1.0%, that most of the descending liquid is transferred into the two phase zone (Equation 4.5).

These calculations are consistent with measurements (Ramey 1970) at the Geysers. In a detailed study, Ramey (1970) identified that at the interface between the liquid and two-phase zone, the porous matrix was composed of a highly impermeable, low porosity shale, with many pore spaces filled with quartz precipitate. However, in the underlying vapor-dominated two-phase region, which is of order 1km deep, the matrix is much more permeable, with porosities of order 5-8% (Pruess and Narasimhan 1982). As may be seen in Figure 4.3, this configuration is stable if the porosity of the impermeable shale layer near the interface is smaller than about 0.5%.

The time-scale for growth of the instability is controlled by the time required for a pressure wave to migrate a distance h_c through the two-phase zone. Small pressure perturbations migrate through the two-phase region with effective diffusivity (Grant and Sorey 1978) $D \approx K/\phi\mu\beta$, and so the time-scale for instability is $\tau \approx h_c^2/D$. For typical geothermal systems, $\tau \approx 10^5 - 10^8$s corresponding to periods of days to a few years. Since geothermal systems evolve over times of order $10^3 - 10^4$years (Grant, Donaldson and Bixley 1982), unstable states are unlikely to be realized in practice. The present analysis therefore imposes very stringent constraints on the possible depths of quasi-steady two-phase zones in geothermal systems.

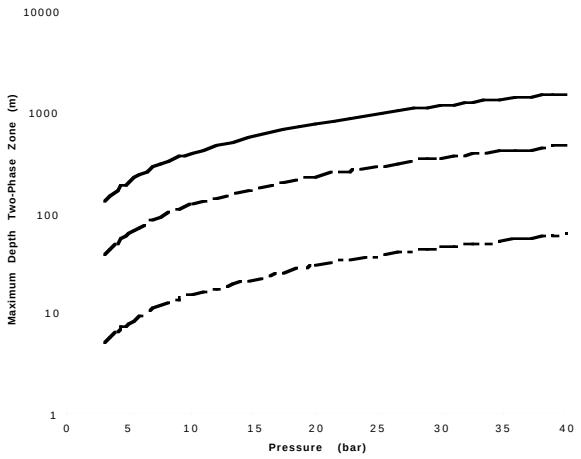

Figure 4.3 The maximum depth of a two-phase zone which may be overlain by a layer of liquid as a function of the reservoir pressure, and hence depth of the upper surface of the two-phase zone. Curves are shown for matrix porosities near the interface of 0.5, 1.0 and 8.0% in accord with the typical range of porosities at The Geysers (Gunderson 1991). Material properties for the vapor are taken from Haywood (1972).

Our model implies that geothermal systems in which liquid overlies an extensive two-phase zone may be relatively rare, since they require a zone of very low porosity and permeability near the interface between the two-phase and liquid regions. No such restriction applies to systems in which a two-phase zone extends to the surface, such as at Yellowstone and Wairakei (Grant, Donaldson and Bixley 1982; White *et al.* 1975; Elder 1981) (Figure 4.1*b*), since there is no overlying liquid to drive a compressional instability of the two-phase zone. Finally, our model identifies that the hydrothermal systems which often develop below active volcanic crater lakes may be intrinsically unsteady, possibly leading to fluctuations of the lake temperature over periods of months to years, as observed at Mt Ruapehu (Christenson and Wood 1991; Hurst *et al.* 1991) during the period 1930-1995, or heating of the lake to temperatures close to the boiling point, as observed at Poas volcano (Brown *et al.* 1989).

4.1.3 Experimental Procedure

In order to verify the prediction of the onset of instability by the simple model, we intend to perform a suite of experiments. Work has commenced on the construction of a heat pipe similar to that used by Bau and Torrance (1982). A 1m high sand pack is heated from the base and a series of thermocouples are placed along the axis of the core. Experiments are scheduled to start within the next few weeks. We hope to test the hypothesis for the theoretical stability criterion developed in the last quarter. In order to do this, we shall use porous medium packs of different material in order to vary the effective compressibility of a two-phase medium.

4.2 NUMERICAL AND EXPERIMENTAL INVESTIGATIONS OF HEAT PIPES IN FRACTURED RESERVOIRS

4.2.1 Current Status

After having constructed a one-dimensional model that conforms with the theoretical model of Bau and Torrance (1982) of a liquid dominated heat pipe, the model was extended and modified to a two-dimensional reservoir scale model. The first model constructed was a 20 x 1 x 14 block model (Fig. 4.2.1). The model is 25 m, 10 m and 500 m in the x, y and z dimensions, respectively. The top of the reservoir is connected to a heat sink which consists of a zero porosity, low permeability rock matrix which extends 250 km in the x direction, 100 km in the y direction and 1 m in the z direction. The second layer is connected to an aquifer which contains water with an enthalpy of 943.51 kJ/kg and a water pressure of 5.0 MPa.

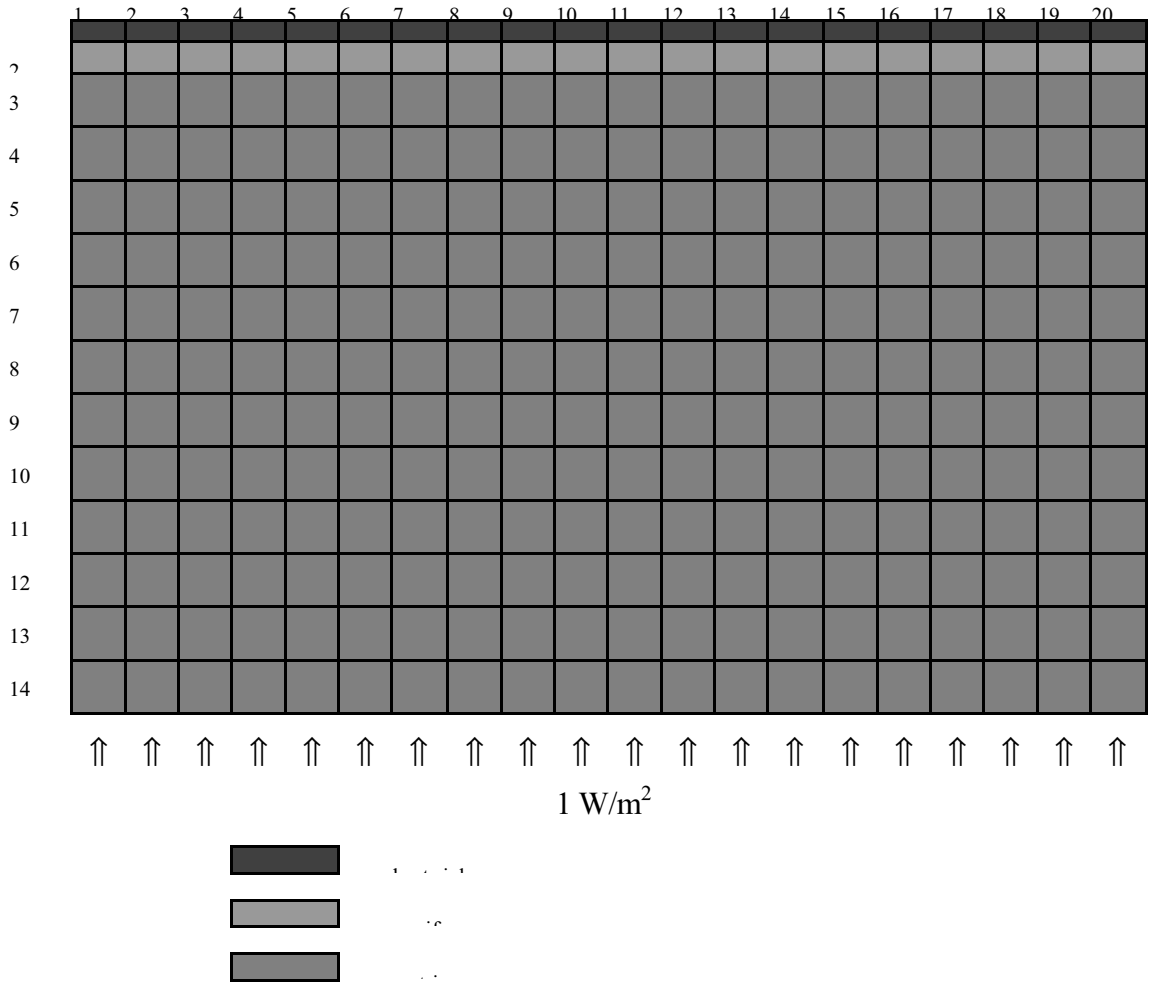

Figure 4.2.1 The 20 x 1 x 14 block model.

The matrix blocks are 1.25 m x 10 m x 40 m with a permeability of 0.003 mD and a porosity of 0.1. The relative permeability curve used was cubic. Initially, the blocks in the first 200 m were fully saturated with water while the rest of the blocks had a water saturation of 0.87. A 1 W/m^2 heat flux was injected through the blocks in layer 14.

A second model similar to the first one was constructed. The only difference between the two models was the grid system used (Fig. 4.2.2). In the second the model, the first 4 blocks have a length of 15.6 mm, the next two have a length of 31.25 mm and the succeeding blocks have increasing lengths until the last one has a length of 10 m. The matrix blocks have been discretized in the z direction such that layers 3 to 11 are 20 m thick, layers 12 to 15 are 50 m thick and layer 16 is 100 m thick.

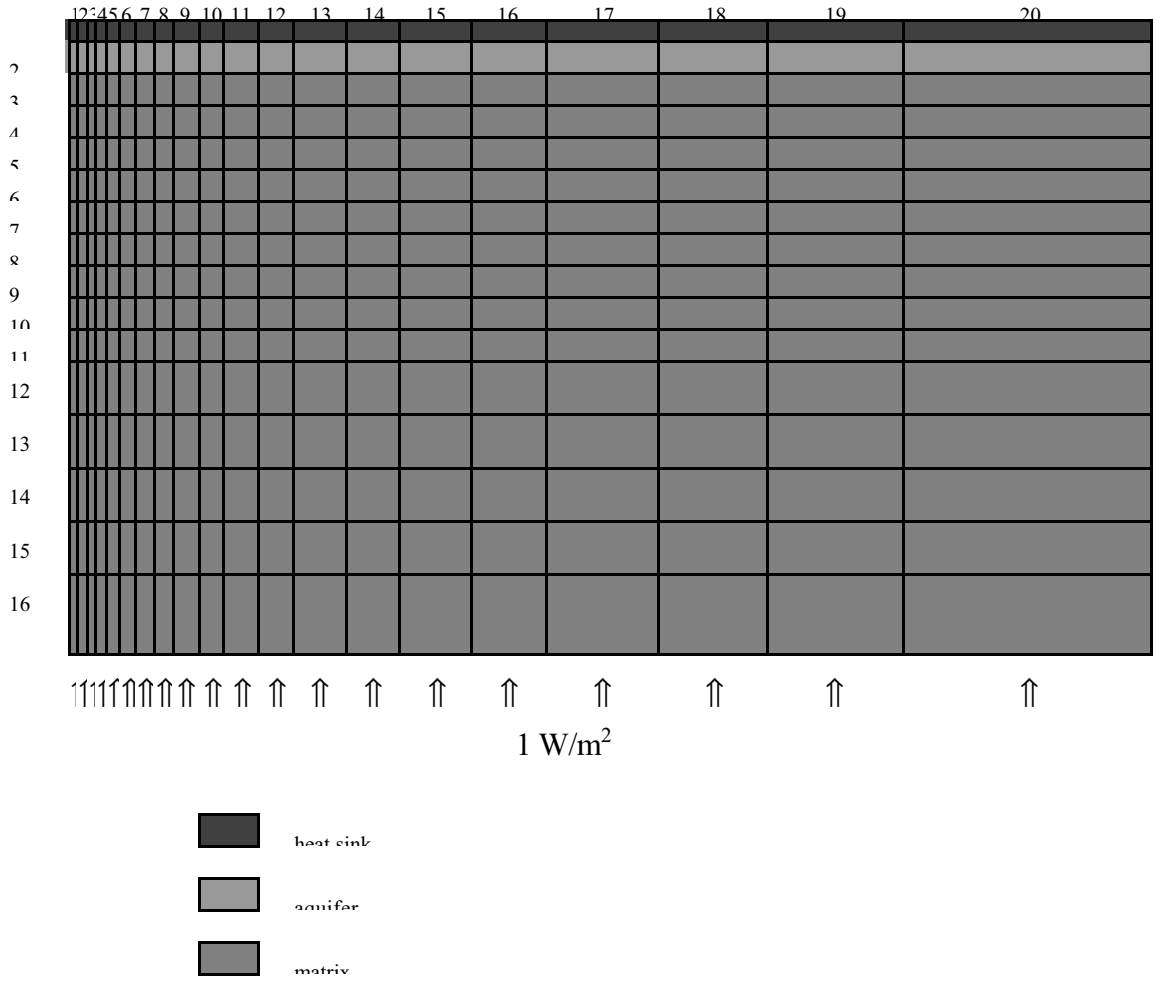

Figure 4.2.2 The 20 x 1 x 16 block model.

The third model constructed was similar to the second one except that the blocks in the first column were given different rock properties. These blocks (Fig. 4.2.3) were given a porosity of 0.5 and a permeability of 300 D in order to model a fracture. Since the numerical simulator TETRAD harmonically averages the permeability, the matrix-fracture interblock permeability is 0.003 mD. For the fracture, we assume a cubic dependence of relative permeability on phase saturation.

The above numerical models were run until steady state solutions were obtained (1.0 x 10^8 days). The steady state solutions were then compared.

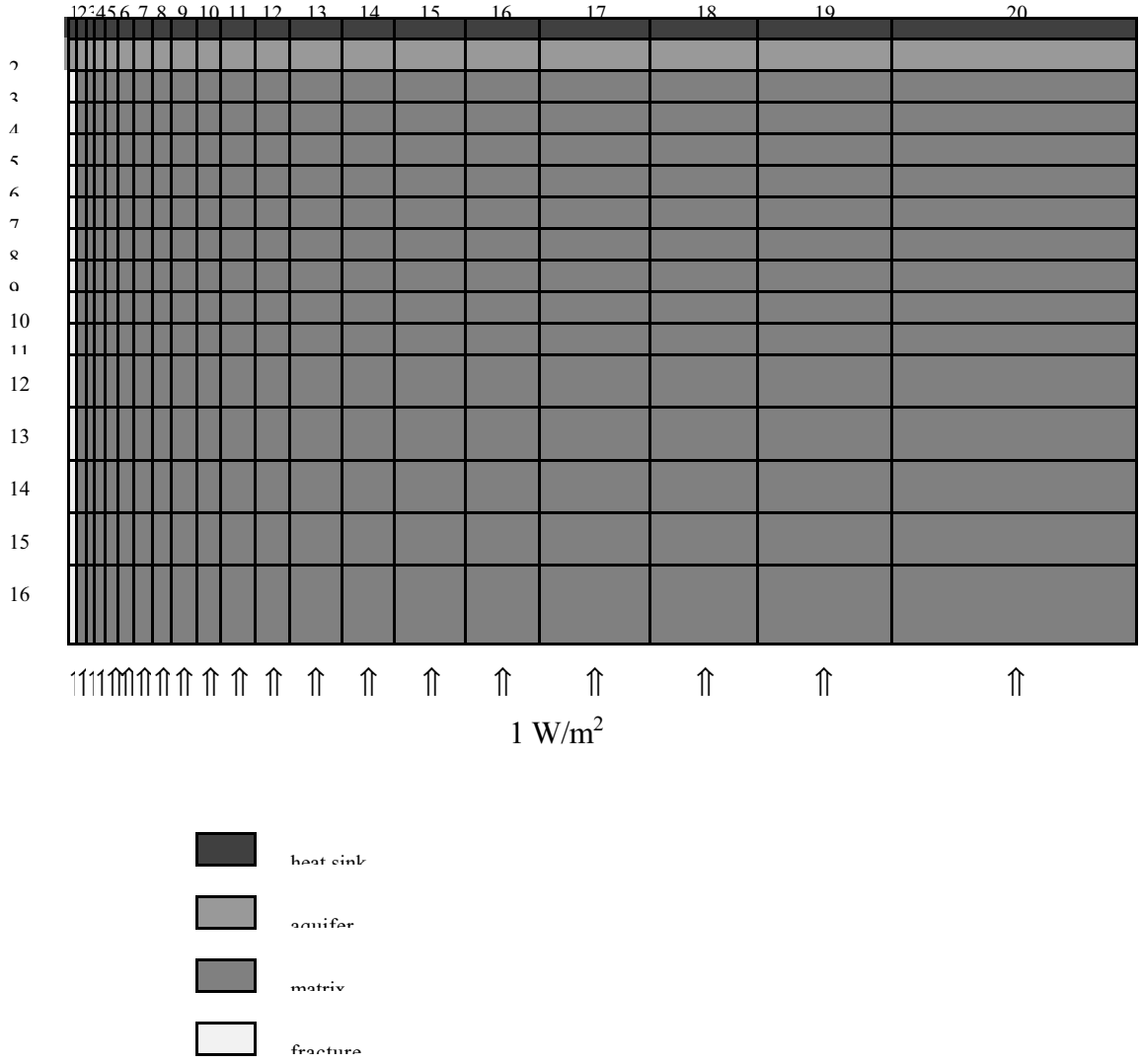

Figure 4.2.3 The 20 x 1 x 16 block model.

4.2.2 Results and Discussion

The only difference between Models 1 and 2 is the kind of grid system utilized. The problem remains the same physically and yet it has been observed that the steady state solutions differ. This is illustrated by Figures 4.2.4 to 4.2.5.

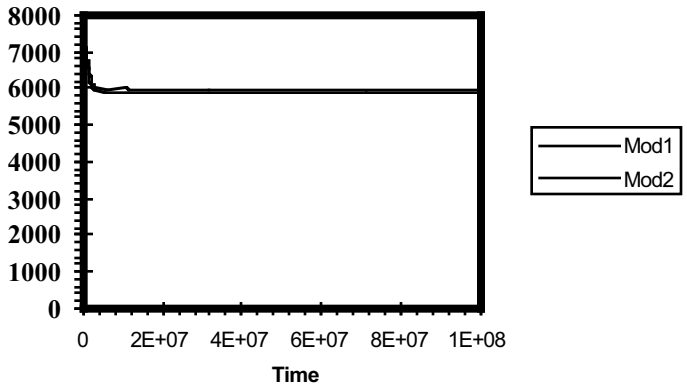

Figure 4.2.4 Pressure history for block 100 (Model 1) and block 160 (Model 2).

Fig. 4.2.4 shows the pressure history and the steady state solution of the two models differ by 81 kPa. Fig. 4.2.5 shows that the steady state solution differs by 3°C. On the other hand, the steam saturation was zero for all time.

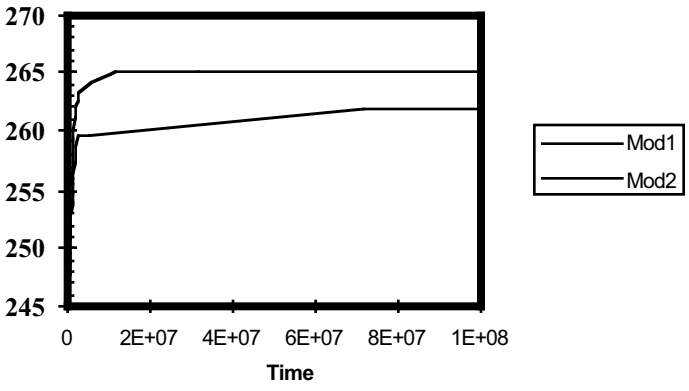

Figure 4.2.5 Temperature history for block 100 (Model 1) and block 160 (Model 2).

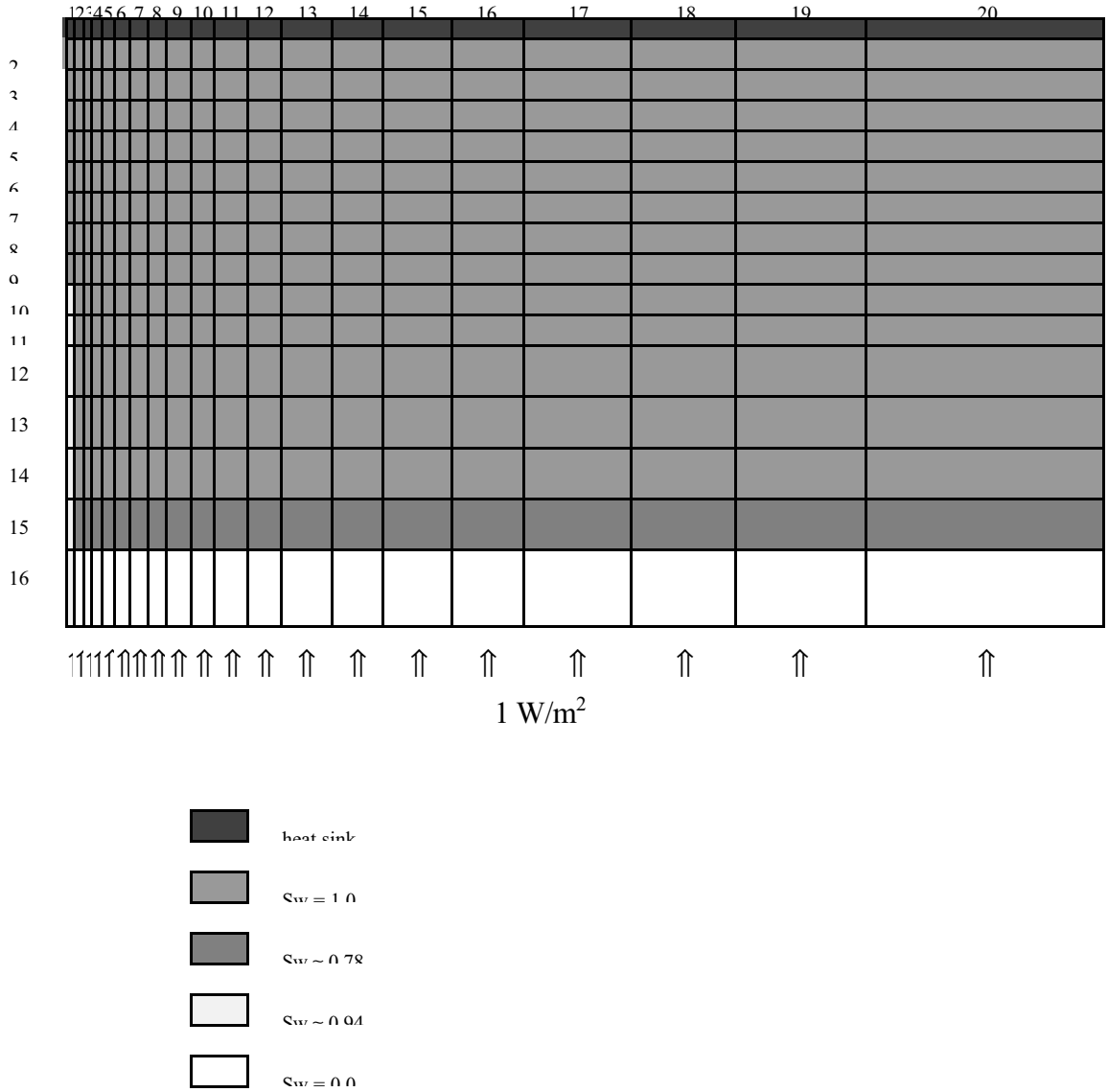

Figure 4.2.6 Water saturation distribution for Model 3.

The different steady state solutions are due to different discretization errors. Model 2 has a finer mesh and therefore has a smaller discretization error than Model 1. Hence, it is important to ensure that the same grid is used whenever the effects of a particular parameter are being investigated.

For Model 3, a steady state solution has been obtained. The water saturation distribution is shown in Figure 4.2.6. The upper boundary remains at a temperature of 220°C while the calculated bottom temperature is 300°C.

4.2.3 Summary

We have observed that the use of different grids result in different steady state solutions even though the physics of the problem remains the same. This discrepancy is due to discretization error differences. Model 2 which had more grid blocks has a smaller discretization error. Due to the influence of the grid, it is imperative that the grid used must remain the same whenever one investigates the effect of a particular parameter on the solution.

Having successfully constructed a two-dimensional model of a fracture-matrix system, in the next quarter we intend to study the effects of capillary forces on the system.

5 REFERENCES

Ambusso, W.J. (1996) Experimental determination of steam-water relative permeability relations. *MS Thesis*, Stanford University, Stanford, CA.

Bau, H. M. and Torrance, K. E. (1982) Boiling in low-permeability porous materials. *Int. J. Heat Mass Transfer* **25,** 45-55.

Bodvarsson, G. (1972) Thermal problems in the siting of reinjection wells. *Geothermics* **1**(2), 63-66.

Bodvarsson, G.S. and Tsang, C.F. (1982) Injection and thermal breakthrough in fractured geothermal reservoirs. *J. Geophys. Res*. **87**(B2), 1031-1048.

Brooks, R.H. and Corey, A.T. (1964) Hydraulic properties of porous media. *Colorado State University, Hydro Paper* No.**5**.

Brown, G., Rymer, H., Dowden, J., Kapadia, P., Stevenson, D., Barquero, J. and Morales, L.D. (1989) Energy budget analysis of Poas Lake *Nature* **339**, 370-373.

Chen, H.K., Council, J.R. and Ramey, H.J. Jr. (1978) Experimental steam-water permeability curves. *GRC Trans*. **2**, 102-104.

Christenson, C.W. and Wood. C.P. (1991) Ruapehu crater lake temperature variations. *Bull. Volc*. **55**, 547-565.

Clossman. P.J. and Vinegar, H.J. (1988) Relative permeability to steam and water at residual oil in natural cores: CT scan saturation. *SPE Paper* **174449**.

Corey, A.T. (1954) The interrelations between gas and oil relative permeabilities. *Producers Monthly* **19**, 38-41.

Counsil, J.R. and Ramey, H.J. Jr. (1979) Drainage relative permeabilities obtained from steam water boiling flow and external gas drive experiments. *GRC Trans*. **3**, 141-143.

Elder, J. (1981) *Geothermal Systems*. Academic Press.

Enedy, S., Enedy, K. and Maney, J. (1991) Reservoir response to injection in the Southeast Geysers. *Proc. Stanford Geoth. Workshop* **16**, 75-82.

Enedy, S.L., Smith, J.L., Yarter, R.E., Jones, S.M. and Cavote, P.E. (1993) Impact of injection on reservoir performance in the NCPA steam field at the Geysers. *Proc. Stanford Geoth. Workshop* **18**, 125-134.

Fitzgerald, S.D., Pruess, K. and van Rappard (1996) Laboratory studies of injection into horizontal fractures. *Proc. Stanford Geoth. Workshop* **21**, 113-118.

Fitzgerald, S.D. and Woods, A.W. (1994) The instability of a vaporization front in hot porous rock. *Nature* **367**, 450-453.

Goyal, K.P. (1994) Injection performance evaluation in Unit 13, Unit 16, SMUDGEO#1, and Bear Cayon areas of the Southeast Geysers. *Proc. Stanford Geoth. Workshop* **19**, 27-34.

Grant, M.A. (1979) Interpretation of downhole measurements in geothermal wells. *Rep. 88 Appl. Math. Div., Dep. Sci. Ind. Res., New Zealand*.

Grant, M.A. (1977) Permeability reduction factors at Wairakei. *Paper presented at AIChE-ASME Heat Transfer Conference, AIChE, Salt Lake City, Utah, August*15-17.

Grant M.A., Donaldson, I.G., and Bixley, P. (1982) *Geothermal Reservoir Engineering*. Academic Press, New York.

Grant, M.A. and Sorey, M.L. (1978) The compressibility of two-phase reservoirs. *Water Resources Res*. **15**, 684-686.

Gunderson, R.P. (1991) Porosity of reservoirs graywacke at The Geysers. Monograph on The Geysers Geothermal Field} *Geothermal Resources Council*, Special Report **17**, 89-93.

Harper, R.T. and Jordan, O.T. (1985) Geochemical changes in response to production and reinjection for Palinpinon-I geothermal field, Negros Oriental, Philippines. *Proc. New Zealand Geothermal Workshop* **7**, 39-44.

Hassler, G.L. (1944) Method and apparatus for permeability measurements. *U.S. Pat. Off*., Washington, D.C., 1944.

Haywood, R.W. (1972) *Thermodynamic tables in SI (metric) units*. Cambridge Univ. Press.

Horne, R.N. (1982) Geothermal reinjection experience in Japan. *J. Petroleum Tech*. **March**, 495-503.

Horne, R.N. and Ramey, H.J., Jr. (1978) Steam/water relative permeabilities from production data. *GRC Trans*. **2**, 291.

Hurst, A.W., Bibby, H.M., Scott, B.J. and McGuinness, M.J. (1991) Heat pipes in volcanoes. *J. Volcan. Geoth. Res*. **46**, 1-20.

Ingebritsen, S.E. and Sorey, M.L. (1988) Vapor-dominated geothermal systems. *J. Geophys. Res*., **93**, 13635-13655.

Johns, J.R., Steude, J.S., Castanier, L.M. and Roberts, P.V. (1993) Nondestructive measurements of fracture aperture in crystalline rock core using X-Ray computed tomography. *J. Geophys. Res.* **98**(B2), 1889-1900.

Klein, C. and Enedy, S. (1989) Effect of condensate reinjection on steam chemistry at The Geysers field. *Trans. Geoth. Res. Counc*. **13**, 409-413.

Mossop, A. (1996) Induced seismicity at The Geysers geothermal field, California I-A thermoelastic injection model. *in prep*.

Nakamura, H. (1981) Development and utilization of geothermal energy in Japan. *Trans. Geothermal Resources Council* **5**, 33-35.

Osoba, J.S., Richardson, J.J., Kerver, J.K., Hafford, J.A. and Blair, P.M. (1951) Laboratory measurements of relative permeability. *Trans. AIME*, **192**, 47-55.

Pruess, K. (1991) *TOUGH User's Guide*. Earth Sci. Div., Report LBL-20700, Lawrence Berkeley Laboratory.

Pruess, K. and Bodvarsson, G.S. (1984) Thermal effects of reinjection in geothermal reservoirs with major vertical fractures. *J. Pet. Tech*. **Sep**, 1567-1578.

Pruess, K., Calore, C., Celati, R. and Wu, Y.S. (1987) An analytical solution for heat transfer at a boiling front moving through a porous medium. *Int. J. Heat Mass Transfer* **30**(12), 2595-2602.

Pruess, K. and Narasimhan, T.N. (1982) On fluid reserves and the production of superheated steam from fractured, vapor-dominated geothermal reservoirs. *J. Geophys. Res*. **87**(B11), 9329-9339.

Ramey, H.J.Jr. (1970) Submitted as evidence, Reich vs. Reich; Petitioners v. Commissioner of Internal Revenue, 1969 Tax Court of the United States, 52. T. C. No. 74.

Sanchez, J.M. (1987) Surfactant effects on the two-phase flow of steam/water and nitrogen/water in an unconsolidated permeable medium. *Ph.D. Thesis*, University of Texas, Austin, Texas.

Satik, C. (1994) Studies in vapor-liquid flow in porous media. *Ph.D. Thesis,* University of Southern California, Los Angeles, CA.

Satik, C., Ambusso, W., Castanier, L.M. and Horne, R.N. (1995) A preliminary study of relative permeability in geothermal rocks. *Trans. GRC,* **19**, 539.

Satik, C. and Yortsos, Y.C. (1996) A pore network study of bubble growth in porous media driven by heat transfer. *J. Heat Transfer,* **118**.

Schubert, G. and Straus, J. M. (1980) Gravitational stability of water over steam in vapor-dominated geothermal systems. *J. Geophys. Res.* **85**(B11), 6505-6512.

Schubert, G., Straus, J.M. and Grant, M. (1980) Why doesn't the water fall down? *Nature* **287**, 423-425.

Sorey, M.L., Grant, M.A. and Bradford, E. (1980) Nonlinear effects in two phase flow to wells in geothermal reservoirs. *Water Resources Research* **16**(4), 767-777.

Sulphur Bank Well Logs, The Geysers (1967-1978) *Calif. Div. Oil, Gas and Geothermal Resources*.

Truesdell, A.H. and White, D.E. (1973) Production of superheated steam from vapor-dominated geothermal reservoirs. *Geothermics* **2**, 154-173.

Verma, M.A. (1986) Effects of phase transformation of steam-water two-phase relative-permeability. *Ph.D. Thesis*. University of California, Berkeley.

Weast, R.C. (1972) *Handbook of Chemistry and Physics*. Chemical Rubber Co.

White, D.E., Fournier, R.O., Muffler, L.J.P. and Truesdell, A.H. (1975) Physical results of research drilling in thermal areas of Yellowstone National Park, Wyoming. *Geological Survey Professional Pap*er **892**.

White, D.E., Muffler, L.J.P. and Truesdell, A.H. (1971) Vapor-dominated hydrothermal systems compared with hot water systems. *Econ. Geol*. **66**, 75-97.

Woods, A.W. and Fitzgerald, S.D. (1993) The vaporization of a liquid front moving through a hot porous rock. *J. Fluid Mech*. **251**, 563-579.

Woods , A.W. and Fitzgerald, S.D. (1996) Laboratory and theoretical models of fluid recharge in superheated geothermal systems. *J. Geophys. Res. in press*

Woods, A.W. and Fitzgerald, S.D. (1997) The vaporization of a liquid front moving slowly through a hot porous rock. Part II *J. Fluid Mech. submitted*